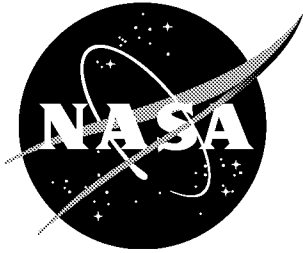


NASA/TM-2001-211263



CFD Sensitivity Analysis of a Modern Civil Transport Near Buffet-Onset Conditions

*Christopher L. Rumsey, Dennis O. Allison, Robert T. Biedron, Pieter G. Buning,
Thomas G. Gainer, Joseph H. Morrison, and S. Melissa Rivers
Langley Research Center, Hampton, Virginia*

*Stephen J. Mysko
The Boeing Company, Long Beach, California*

*David P. Witkowski
The Boeing Company, Seattle, Washington*

December 2001

The NASA STI Program Office ... in Profile

Since its founding, NASA has been dedicated to the advancement of aeronautics and space science. The NASA Scientific and Technical Information (STI) Program Office plays a key part in helping NASA maintain this important role.

The NASA STI Program Office is operated by Langley Research Center, the lead center for NASA's scientific and technical information. The NASA STI Program Office provides access to the NASA STI Database, the largest collection of aeronautical and space science STI in the world. The Program Office is also NASA's institutional mechanism for disseminating the results of its research and development activities. These results are published by NASA in the NASA STI Report Series, which includes the following report types:

- **TECHNICAL PUBLICATION.** Reports of completed research or a major significant phase of research that present the results of NASA programs and include extensive data or theoretical analysis. Includes compilations of significant scientific and technical data and information deemed to be of continuing reference value. NASA counterpart of peer-reviewed formal professional papers, but having less stringent limitations on manuscript length and extent of graphic presentations.
- **TECHNICAL MEMORANDUM.** Scientific and technical findings that are preliminary or of specialized interest, e.g., quick release reports, working papers, and bibliographies that contain minimal annotation. Does not contain extensive analysis.
- **CONTRACTOR REPORT.** Scientific and technical findings by NASA-sponsored contractors and grantees.

- **CONFERENCE PUBLICATION.** Collected papers from scientific and technical conferences, symposia, seminars, or other meetings sponsored or co-sponsored by NASA.
- **SPECIAL PUBLICATION.** Scientific, technical, or historical information from NASA programs, projects, and missions, often concerned with subjects having substantial public interest.
- **TECHNICAL TRANSLATION.** English-language translations of foreign scientific and technical material pertinent to NASA's mission.

Specialized services that complement the STI Program Office's diverse offerings include creating custom thesauri, building customized databases, organizing and publishing research results ... even providing videos.

For more information about the NASA STI Program Office, see the following:

- Access the NASA STI Program Home Page at <http://www.sti.nasa.gov>
- E-mail your question via the Internet to help@sti.nasa.gov
- Fax your question to the NASA STI Help Desk at (301) 621-0134
- Phone the NASA STI Help Desk at (301) 621-0390
- Write to:
NASA STI Help Desk
NASA Center for AeroSpace Information
7121 Standard Drive
Hanover, MD 21076-1320

NASA/TM-2001-211263



CFD Sensitivity Analysis of a Modern Civil Transport Near Buffet-Onset Conditions

*Christopher L. Rumsey, Dennis O. Allison, Robert T. Biedron, Pieter G. Buning,
Thomas G. Gainer, Joseph H. Morrison, and S. Melissa Rivers
Langley Research Center, Hampton, Virginia*

*Stephen J. Mysko
The Boeing Company, Long Beach, California*

*David P. Witkowski
The Boeing Company, Seattle, Washington*

National Aeronautics and
Space Administration

Langley Research Center
Hampton, Virginia 23681-2199

December 2001

Available from:

NASA Center for AeroSpace Information (CASI)
7121 Standard Drive
Hanover, MD 21076-1320
(301) 621-0390

National Technical Information Service (NTIS)
5285 Port Royal Road
Springfield, VA 22161-2171
(703) 605-6000

Contents

ABSTRACT	iv
TERMS, SYMBOLS, AND ABBREVIATIONS	v
1 INTRODUCTION	1
1.1 Current CFD Capabilities and Known Limitations	2
1.2 Rationale for Work Performed	4
1.3 How this Document is Organized	6
2 METHODOLOGY	7
2.1 Previous Studies and Factors that Influenced the Current Methodology	7
2.2 Description of CFD Codes	9
2.3 Description of Turbulence Models	9
2.4 Description of Grids	10
2.5 Summary of Computations Performed	15
2.6 Summary of Current “Best Practices”	15
3 CFD SENSITIVITY ANALYSIS	18
3.1 Effect of Grid	18
3.2 Effect of Code and Spatial Differencing Method	21
3.3 Effect of Aeroelastic Shape	23
3.4 Effect of Turbulence Model	26
3.5 Summary of CFD Sensitivities	28
4 COMPARISONS WITH WIND TUNNEL DATA	31
5 COMPARISONS WITH FLIGHT DATA	43
5.1 Discussion on Flight Data	43
5.2 Comparisons	45
6 SUMMARY	48
7 CONCLUDING REMARKS	50
ACKNOWLEDGMENTS	51
APPENDIX A: INDUSTRY PERSPECTIVE ON CFD	52

ABSTRACT

A CFD sensitivity analysis is conducted for a modern civil transport at several conditions ranging from mostly attached flow to flow with substantial separation. Two different Navier-Stokes computer codes and four different turbulence models are utilized, and results are compared both to wind tunnel data at flight Reynolds number and flight data.

In-depth CFD sensitivities to grid, code, spatial differencing method, aeroelastic shape, and turbulence model are described for conditions near buffet onset (a condition at which significant separation exists). In summary, given a grid of sufficient density for a given aeroelastic wing shape, the combined approximate error band in CFD at conditions near buffet onset due to code, spatial differencing method, and turbulence model is: 6% in lift, 7% in drag, and 16% in moment. The biggest two contributors to this uncertainty are turbulence model and code.

Computed results agree well with wind tunnel surface pressure measurements both for an overspeed “cruise” case as well as a case with small trailing edge separation. At and beyond buffet onset, computed results agree well over the inner half of the wing, but shock location is predicted too far aft at some of the outboard stations. Lift, drag, and moment curves are predicted in good agreement with experimental results from the wind tunnel.

The current effort was motivated by a problem identified by the U.S. aircraft industry: that state-of-the-art CFD (specifically, Reynolds-averaged Navier-Stokes with current turbulence models) cannot adequately or consistently predict the onset and progression of separated flows. In particular, a specific problem was identified: CFD (and wind tunnel experiment) has predicted lower buffet lift levels than experienced in flight for two particular aircraft. However, in the current investigation, the problem of CFD being unable to achieve flight buffet levels did *not* occur. Instead, the predicted lift curve from CFD tracked the trend from flight data well through buffet all the way to near maximum lift.

TERMS, SYMBOLS, AND ABBREVIATIONS

A	effects due to tunnel model aeroelastics
AST	advanced subsonic transport
ASTAC	AeroSpace Technology Advisory Committee
B	wingspan ($2y/B$ signifies span location)
BB	Baldwin-Barth turbulence model
BL	Baldwin-Lomax turbulence model
BO	buffet onset: $\alpha = 2.8^\circ$ at $M = 0.87$
BO+	slightly above buffet onset α
BO-	slightly below buffet onset α
BOF	buffet onset condition in flight: $\alpha \approx 5.1^\circ$ at $M = 0.87$
C	CFL3D; also effects due to code/differencing
CFD	computational fluid dynamics
DNS	direct numerical simulation
EASM	explicit algebraic stress turbulence model
ETW	European Transonic Windtunnel
FDS	Roe's flux difference-splitting
FF	far field extent
FL	derived from flight tests
FSF	flap support fairing
G	effects due to grid size
LES	large eddy simulation
MAC	mean aerodynamic chord
NTF	National Transonic Facility
O	OVERFLOW
OC	overspeed "cruise" (1-g condition): $\alpha = 1.03^\circ$ at $M = 0.87$
RANS	Reynolds averaged Navier-Stokes
SA	Spalart-Allmaras turbulence model
SA-Ia	Spalart-Allmaras turbulence model, version Ia
SS	small separation: $\alpha = 1.5^\circ$ at $M = 0.87$
SST	Menter's shear stress transport turbulence model
T	effects due to turbulence model
TU	derived from wind tunnel tests
VG	vortex generator
d	distance from the nearest wall
k	turbulent kinetic energy
y	spanwise distance
α	angle of attack
ε	turbulent dissipation rate
ω	specific dissipation rate
Ω	vorticity magnitude
$\hat{S}, \hat{\nu}, \chi, f_{v1}, f_{v2}, f_{v3}, \kappa, C_{v2}$	terms and constants in SA model

1 INTRODUCTION

In the last 20 years, computational fluid dynamics (CFD) has progressed from solving flows over 2-D airfoils to the point of being routinely used for predicting flows over high-Reynolds-number 3-D complex-configuration aerospace vehicles. Although much of this progress is due to dramatic increases in computer speed and memory, the CFD codes and grid generation techniques also have improved in their ability to represent increasingly complex configurations through multi-block (patched or overset) and unstructured-grid methodologies. Also, algorithm advances such as multigrid, low-Mach-number preconditioning, and parallel processing have made their way into most widely-used production CFD codes.

Turbulence modeling for aerospace configurations has also made significant progress. In the early to mid 1990's, the Menter shear-stress-transport (SST) two-equation model [1] and the Spalart-Allmaras (SA) one-equation model [2] were developed, and quickly replaced algebraic models such as the Baldwin-Lomax (BL) model [3] and other two-equation models such as Wilcox's $k-\omega$ model [4] as industry standards. In spite of the fact that they contain many heuristic elements, the SST and SA models improve predictions significantly for a wide variety of 2-D and 3-D experiments involving separated flow, and also generally perform as well as the earlier models for attached flows.

In the last seven years, significant progress has also been made in turbulence modeling with the explicit algebraic stress model (EASM) [5]. The EASM, which contains nonlinear terms, is derived directly from the full Reynolds stress equations and therefore inherently contains more turbulence physics than models built from "the bottom up." It has progressed to the point where it can now be routinely employed for complex configurations [6]. Full Reynolds stress models, which require the solution of seven additional equations, have not reached the point of being robust enough to run easily and routinely for complex flows. Outside the realm of Reynolds-averaged Navier-Stokes, large-eddy simulations (LES) and direct numerical simulation (DNS) require huge increases in computer capacity before they will be usable for high-Reynolds-number complex flows.

Although much progress has been made in CFD, the current state-of-the-art is far from perfect. The aerospace industry is beginning to utilize CFD and trust its results and/or trends near design conditions when there is little or no separated flow; but there is currently little confidence in CFD's ability to predict flows involving significant amounts of separation.

In October 1999, a Boeing-proprietary talk was presented at NASA Langley Research Center titled "CFD Successes and Challenges." In this talk, a variety of cases – mostly for wing-alone, wing-body, or full aircraft configurations – were used to illustrate areas where (from the perspective of industry) state-of-the-art CFD does well and where it is lacking. Several relevant points from this talk are summarized in Appendix A.

As a result of this talk, and in order to address similar concerns raised by the Airframe Systems subcommittee of NASA's AeroSpace Technology Advisory Committee (ASTAC) (formed to review and advise NASA'S Office of Aerospace Technology), NASA Langley and Boeing formed a team to assess CFD capability for aircraft near buffet onset. On a civil aircraft, buffet onset is defined as the condition for which flow field unsteadiness causes the aircraft to shake near the pilot's seat with an acceleration greater than some specified limit (e.g., ± 0.05 g's).

The team was named the "CFD Buffet Onset Team." This report details their results and conclusions for the specific task of determining the sensitivities due to grid, turbulence model, and code for a modern twin-engine civil transport aircraft in buffet/separated conditions. The

reasons and history behind selecting this particular case are detailed in section 1.2. As a part of this effort, comparisons were made with experimental data from the National Transonic Facility (NTF), as well as with flight test data.

1.1 Current CFD Capabilities and Known Limitations

The purpose of this section is to discuss some of the capabilities and known limitations of CFD, in particular applied to complex configurations. It is given as background for the current study of the modern civil transport aircraft, in order to provide some insight into the methodologies chosen and uncertainties involved in the computations.

Use of the Reynolds-averaged Navier-Stokes (RANS) equations implies that the turbulent flow can be represented by a mean state. For stationary turbulence (a turbulent flow that does not vary in time on average), this is generally considered to be a good approximation. However, for unsteady flows (a flow that *does* vary in time), the use of the RANS equations is more questionable. Certainly, unsteady flows must be solved time-accurately, rather than in “steady-state” mode (where different regions of the flow field are advanced at different time steps in order to reach the end result more rapidly). In time-accurate cases, the time scale of the gross unsteady motion should be greater than the physical time step employed in the computations, which in turn should be much greater than the time scales associated with the turbulence. Many good predictions for unsteady turbulent flows have been obtained with time-accurate RANS (see, e.g., Rumsey et al.[7], Wang et al.[8]). But the ability to predict unsteady flows depends on many factors, such as the unsteady time scale(s) and the type of unsteadiness. Much more work needs to be done to define the ranges of unsteady flow conditions for which time-accurate CFD using RANS can be employed.

A flow field of an aerospace-type vehicle can be characterized in terms of three general categories: attached, mildly separated, and massively separated. When a flow field is steady and contains either no separation or mild separation, the RANS equations, closed with one of the “state-of-the-art” turbulence models such as SST or SA and solved to steady state, can often predict the flow field in good agreement with experiment. However, when massive separation exists, results tend to be more dubious. One reason for this uncertainty is that the more massively separated a flow, the more inherently unsteady it is. Unfortunately, the dividing line between “mildly separated” and “massively separated” is vague, and CFD sometimes yields fully-converged steady flow fields even when the flow fields contain fairly large separated regions that in reality are most certainly unsteady. Although this computed steadiness can be attributed to inadequate grid density in many cases, the bottom line is that CFD’s success depends upon the particular case. In some cases, in the mean, a steady separated region predicted by CFD can be a good approximation to the time-averaged unsteady separated region in reality.

Assuming that the use of the RANS equations is appropriate for a particular case, CFD’s capability to represent reality is influenced by three factors: numerical errors, geometric fidelity, and modeling errors.

NUMERICAL ERRORS

Numerical errors arise from the combined effects of the grid and numerical scheme. The grid must be fine enough such that discretization errors for the particular scheme employed are at acceptably low levels. The issue of grid size is not as straightforward to treat as it might at first appear, however. Particularly for complex 3-D configurations, it is very difficult to perform a meaningful grid sensitivity study because achieving a significant increase in grid refinement is

often impractical due to computer limitations. And, in 3-D, the grid sizes necessary to resolve all important features may be so fine that such sufficient grid resolution is difficult to achieve.

For example, it is now well-known that the streamwise grid spacing near the trailing edge of some transonic wings can have a significant effect on the predicted shock location (see, e.g., Garner et al.[9]). If an initial grid has *no* clustering in this region, then small levels of refinement may incorrectly indicate sufficient grid convergence. Only by dramatically refining the grid in the trailing edge region is the feature adequately resolved and the shock position grid converged. For turbulent flows, it is also important to have adequate grid resolution in the sub-layer of the turbulent boundary layer near walls. If certain regions do not, then particular features may not be captured, and small levels of refinement may fail to show any effect.

Grid quality has an often dramatic influence on the CFD solution. Nonorthogonality and high levels of stretching or non-smoothness in the grid can lower the accuracy of the numerical method. If a poor grid is localized to a particular region, then it is possible for a scheme to converge locally with lower order accuracy than in other regions of the flow field. This locally lower accuracy could cause CFD to poorly predict a particular feature that may have a global effect in the solution. The problem of poor grid quality particularly manifests itself in structured grids for complex 3-D configurations. In these cases, grid generation can be difficult because structured grids are often ill-suited to fitting “smoothly” around configurations with many twists, turns, and corners.

GEOMETRIC FIDELITY

Geometric fidelity is the fidelity with which the CFD grid models the actual configuration (whose data the CFD results are being compared to). This issue is very broad, and is the area for which the greatest amount of user insight and experience is often required. Rarely is a CFD analysis made with the *exact* same configuration as experiment or flight test. Usually, simplifications are purposefully made; e.g., ignoring tunnel walls, small components, mounting hardware, etc. For example, the flap support fairings (FSFs) on aircraft are often ignored in the CFD grid because their effects tend to be only manifested locally. The more complex the configuration, usually the more simplifications are made. Care must be exercised to insure that a particular component omitted or simplified in the CFD grid is truly not important or has little effect. As an example, Rogers et al.[10] described how a very small gap between the Krueger slat and the inboard slat of a Boeing 777 in landing configuration was difficult to model faithfully in a CFD grid. In the wind tunnel model, the gap was partially sealed using wax and tape. In spite of its apparent insignificance, different gap treatments in the CFD grid had dramatic effects on the flow over part of the wing. Without the partial sealing of the gap, a vortex formed through the small gap and caused a large stall region on top of the wing. With the sealing, the stall region was reduced considerably and the overall lift coefficient increased by about 3%.

Sometimes, CFD can yield poor predictions because the shape of the body in the grid does not match the actual shape due to unaccounted-for aeroelastic deflections or even differences between theoretical-shape and as-built-shape. Also, how a blunt wing trailing edge is handled in the CFD simulation (brought to a point, left as an “open” gap, or closed) can have a significant effect on the solution, particularly for transonic conditions. This factor is discussed in greater detail in section 2.1.

MODELING ERRORS

Modeling errors are errors that result from an incorrect or incomplete model or theory. The most significant source of modeling error in most CFD computations is the turbulence model. The choice of turbulence model (which can also include a transition model) invariably affects the result of any CFD calculation to some degree. Earlier in the introduction, recent advances in turbulence modeling were discussed. It is clearly acknowledged that all models are imperfect and no model works well for all situations. However, it is often difficult to isolate *specific* failings of a given model because the cases where it fails are often so complex that one cannot easily separate cause and effect. Also, as discussed above, the more complex the configuration, the more uncertainty there is in the numerics and geometric fidelity. So it is often difficult, in the case of complex configurations, to be sure that a given poor prediction is *necessarily* a failure of the turbulence model, and not due instead to one or both of the other factors.

At this point it is important to also mention experiment and flight test. CFD is often compared with wind tunnel or flight measurements as if the measurements were indisputable. Clearly, uncertainties and errors present in the measured data should be accounted for just as in the CFD.

1.2 Rationale for Work Performed

The CFD Buffet Onset Team is comprised of the authors of this report. Initially, the team was presented with the problem (included in the summary in Appendix A) that CFD and high Reynolds number wind tunnel data generally agree with each other for certain modern aircraft (including a modern tri-engine civil transport and a high-wing transport), but both underpredict lift levels present in flight near buffet. Some results are also detailed in Clark and Pelkman [11]. The industry perspective (see Appendix A) maintained that disagreement between CFD and flight was due to inadequate turbulence models for separated high-Reynolds number flows, and that disagreement between wind tunnel and flight was due to tunnel turbulence and model dynamics at high dynamic pressures.

There was also data for the current civil transport aircraft under study (see Fig. 1) that indicated that the C_L at buffet derived from NTF tunnel tests is low compared to C_L at buffet for flight, particularly at overspeed Mach numbers. (ΔC_L is approximately 0.03 at cruise Mach number and approximately 0.10 at an overspeed Mach number of $M = 0.87$.) However, it should be noted that the C_L at buffet for flight is determined by measuring accelerations on the aircraft, whereas the C_L at buffet for the wind tunnel is determined with a proprietary method that makes use of measured force data, as calibrated with previous aircraft. It is not clear whether it is consistent to make comparisons of buffet lift levels using these two completely different methods.

Based on the original problem specification, the preliminary goal established by the team was: *to answer the question why CFD and NTF experiments agree with each other yet disagree with flight near buffet*. However, the issue of flight data “rigidification” soon became a source of entanglement. The rigidification process is used to alter the flight data for direct comparison with the shapes tested in wind tunnels or modeled in CFD. It is generally a linear correction procedure that alters the original data in such a way that the behavior of a rigid wing is mimicked. However, because the method is only an approximation, it is not clear how appropriate it is for comparing to wind tunnel data or CFD.

It was recognized that the team could not resolve these issues associated with the rigidifi-

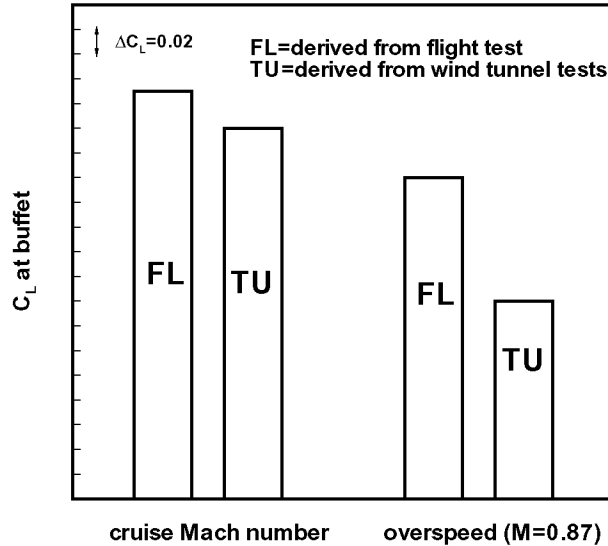


Figure 1: Buffet boundary comparisons for flight vs. correlation method derived from wind tunnel test.

cation process. As a result, the team modified its goal to one that could be accomplished, and that would help to answer some of the questions regarding CFD uncertainty for computations near buffet. The team decided to use a modern twin-engine civil transport aircraft as the vehicle for determining CFD sensitivities. The reason for this choice was: (a) the aircraft possesses a modern aft-loaded wing, (b) on-going NTF tests are being conducted on the aircraft, allowing for concurrent CFD and wind tunnel investigations, and (c) needed aeroelastic shapes are more readily available for this aircraft than others, because it is a current production fleet aircraft. The new goal became:

Establish the sensitivities due to grid, turbulence model, and code for a modern civil transport in buffet/separated conditions.

(Subsequently, sensitivities due to spatial differencing method and aeroelastic shape were also considered.)

The team recommended that rigidified flight data be avoided, and that the correct aeroelastic shapes be used for the wings whenever possible. Data (Fig. 1) indicated that the C_L at buffet predicted using wind tunnel data was fairly close to C_L at buffet for flight at the cruise Mach number, but that at higher Mach numbers there was a more significant difference. Therefore the team decided to focus its attention on computations at the overspeed condition of $M = 0.87$. It was also decided to run three distinct conditions at this Mach number: an overspeed “cruise” condition (OC) case (which is more appropriately referred to as a maximum operating Mach number) with little or no separation, a “small separation” (SS) case, and a “buffet onset” (BO) case with a significant amount of separation. These three conditions were determined from correlations using measured wind tunnel data. The majority of the effort was directed to the buffet onset case.

Although aeroelastic data is available for the wind tunnel model using photogrammetry [12],

measurements do not exist for the flight vehicle’s aeroelastic wing shape in flight. However, in an effort to get a rough idea of the role of the aeroelastics between the wind tunnel model and flight vehicle, an *estimated* flight shape for the buffet onset condition in flight (BOF) was obtained from a loads analysis. Further discussion of the BOF shape is given in sections 2.4 and 3.3.

Details of the grid methodology are given in section 2.4. A series of 27 CFD runs were performed and analyzed by the team. These runs are summarized in section 2.5.

1.3 How this Document is Organized

Section 2 describes the methodology used for the current study. The rationale behind some of the choices made by the team is given, and a summary of the team’s “best practices” is listed. The sensitivity results are given in section 3, for CFD alone. This is followed in section 4 by comparisons with wind tunnel data, and in section 5 by comparisons with flight data. The final two sections give a summary and conclusions.

2 METHODOLOGY

2.1 Previous Studies and Factors that Influenced the Current Methodology

Several previous studies, both published and unpublished, have influenced the team's choice of methodology. One issue of importance is the treatment of a blunt wing trailing edge. Several strategies have been attempted by others. Some possible strategies are illustrated schematically in Fig. 2. These strategies include (a) altering the trailing edge to a point, (b) leaving the wake cut of the grid "open," (c) closing the wake cut over one grid point, and (d - f) modeling the actual blunt trailing edge with various grid closures. Most of these previous trailing edge treatment studies are unpublished, or are only given in company-internal reports. Jiang [13] has a brief discussion of the differences between leaving the wake cut "open" and inserting a grid zone in the wake cut.

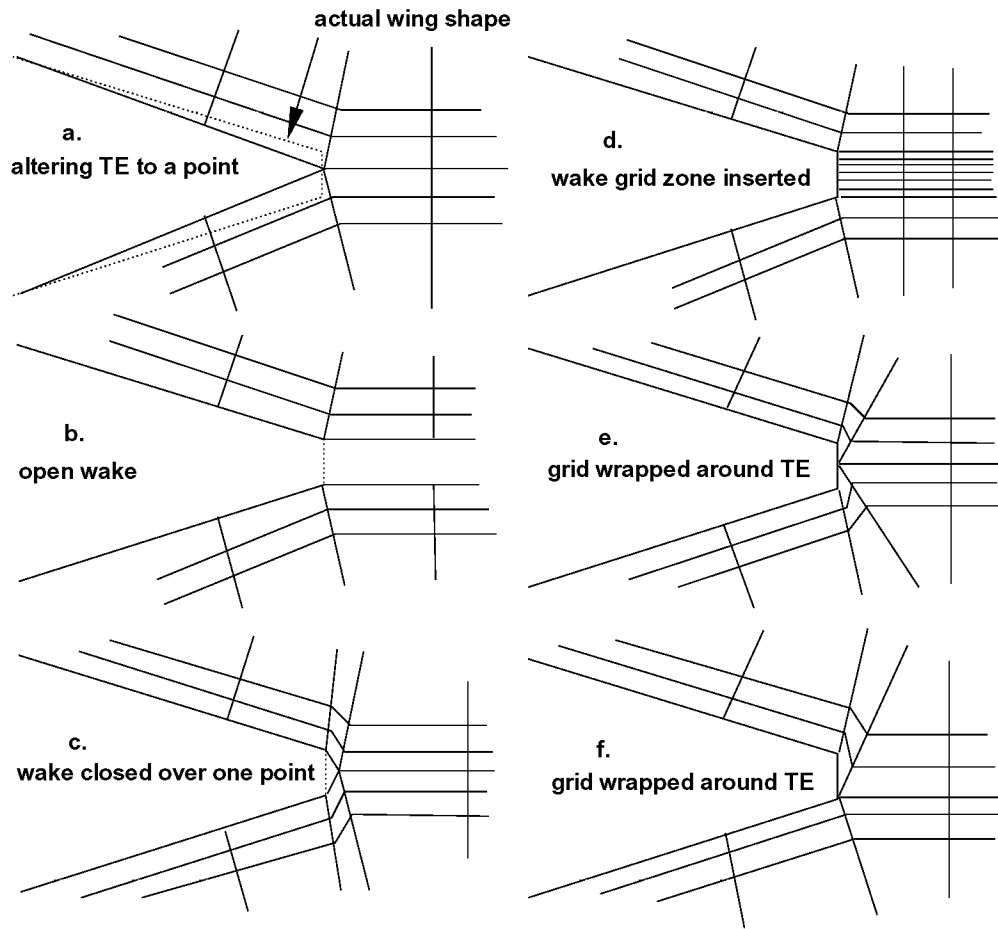


Figure 2: Schematic of some blunt wing trailing edge grid treatments (only a few sample grid lines are shown for clarity).

The treatment of a blunt wing trailing edge can have a significant effect on the shock location for transonic computations, particularly when the flow near the trailing edge is attached.

However, unpublished results suggest that more accurately modeling the base shape may have a tendency to cause the computations to go locally unsteady (the computations correctly try to resolve unsteady shedding off the corner of the blunt base). When a flow has a tendency to go unsteady, it needs to be run time-accurately rather than in steady-state mode, in order to capture the correct physics. But this can be very costly and time consuming, and its benefit for global studies in which forces and surface pressures are of primary concern is questionable.

A preliminary study by this team used two different grids for the aircraft at cruise conditions. One grid used one-to-one multi-block interfaces, and had a trailing edge grid closed over one point, strategy (c) (in Fig. 2). The trailing edge itself had a thickness comparable to the NTF model. The second grid used overset multi-block interfaces, and had an “open” wake cut, strategy (b) (in Fig. 2). Its trailing edge thickness was comparable to the flight aircraft (smaller than that of the wind tunnel model). The two grids produced a surprisingly large difference in predicted shock location (of between 5 and 10 % local chord) at the outboard stations. The resulting lift coefficients for the aircraft were different by 6%, drag coefficient by 6%, and moment by 13%. On the other hand, code-to-code differences on an identical grid were very small.

After analysis, no single factor could be isolated as the cause of the differences. The three factors: wake treatment, trailing edge thickness, and grid topology all played significant roles. In other words, geometric fidelity in combination with numerical issues associated with the grid topology were all sources of error.

As a result of this early study, and taking into account other proprietary studies done previously, the team decided to model the NTF model’s shape (i.e., the trailing edge thickness corresponds with the wind tunnel model thickness) with the trailing edge wake closed over one grid point, strategy (c) (in Fig. 2). This option seemed to be the best compromise between faithfully modeling the tunnel model’s trailing edge and ensuring that the solutions would not have a tendency to go unsteady. Also, an overset grid approach was chosen, because of its generally higher quality compared to the one-to-one methodology.

A variety of engine inflow/outflow boundary condition treatments have been employed previously in industry. One approach is to specify information on both the engine inflow face and on the engine exhaust face(s), and not compute flow through the engine itself. For an aircraft engine, this is the only realistic choice available: the interior of the engine is treated as a “black box.” When modeling wind tunnel models for which the engine is “flow through” (has nothing in its interior and allows flow through it), a second approach is to grid the model’s nacelle interior and compute the actual flow through it. In other words, computing with flow-through implies that no boundary condition specification is necessary at the engine faces. For this study, the flow-through method is employed. Engine power effects are not considered here because secondary jet effects are believed to have negligible effect on buffet for the current configuration, based on proprietary jet effects wind tunnel tests.

Two limited exclusive rights progress reports from NASA’s AST program [14, 15] described the effect of wind tunnel walls on the CFD solution for models in the NTF. Boundary conditions were developed to simulate the tunnel’s slotted walls. Results for several configurations both near cruise and near buffet conditions showed that using CFD with “free-air” grids (extending to the far field) give very good agreement compared to CFD runs in which the slotted walls are modeled. Based on these reports, the team decided to use only “free-air” grids for the current investigation, and avoid the complicating factor of trying to apply the same slotted wall boundary condition in two different codes.

The flight vehicle has vortex generators (VGs) on the wing upper surface to help delay stall and improve performance near buffet, particularly at overspeed conditions. It is known that the VGs promote the transfer of momentum across the boundary layer and delay or eliminate separation. NTF tests included evaluation of VG increments. Furthermore, the flight vehicle possesses flap support fairings (FSFs) on each wing; the wind tunnel model was evaluated both with and without these as well. For the CFD study, the wind tunnel configuration without VGs or FSFs is modeled. Including either of these items increases the complexity and size of the grid, thus requiring additional time both for grid generation and for the CFD computations. Unpublished computations have been performed at Boeing-Seattle using the current aircraft configuration with VGs and FSFs. Although not shown in this report, these unpublished results are consistent with the current results and support the conclusions made herein.

Previous unpublished studies showed that having a large sting support extending from the back end of the fuselage could have a significant effect on the wing pressures (particularly the shock location) at transonic cruise conditions (see Appendix A). However, the current model is mounted on a blade mount modeled after the vertical tail, but thickened for strength. This mounting reduces interference with fuselage up-sweep, and the sting is also located farther from the wing than a fuselage mount. The current study assumes that the tail-mounted sting effects are very small, and uses a grid with no tail or sting. The effects of ignoring the tail-mounted sting are not known, and a study of the effect of tail-mounted sting was deferred.

2.2 Description of CFD Codes

Two different CFD codes were employed in this study: CFL3D [16] and OVERFLOW [17]. Both codes were developed at NASA. Both are multi-zone codes in wide use in U.S. industry. Both can use overset grids, and both employ local time step scaling, grid sequencing, and multigrid to accelerate convergence to steady state. Time-accurate modes are also available for both codes, and both can employ low-Mach number preconditioning for accuracy in computing low-speed steady state flows.

CFL3D is a finite volume method. It uses third-order upwind-biased spatial differencing on the convective and pressure terms, and second-order differencing on the viscous terms; it is globally second-order spatially accurate. The flux difference-splitting (FDS) method of Roe is employed to obtain fluxes at the cell faces. It is advanced in time with an implicit three-factor approximate factorization method.

OVERFLOW is a finite difference method. It can use either second-order central differencing or third-order FDS. Left-hand side options include a diagonalized (scalar pentadiagonal) scheme and an LU-SGS scheme. First-order implicit time advancement is used.

For this study, both CFL3D and OVERFLOW employed the PEGSUS [18] software to obtain overset interpolants for the regions of overlapping grid.

2.3 Description of Turbulence Models

Three state-of-the-art turbulence models were selected for the current study. These are: Spalart-Allmaras (SA) [2], Menter's shear stress transport (SST) $k-\omega$ [1], and an explicit algebraic stress model (EASM) in $k-\omega$ form [6]. A fourth model, Baldwin-Barth (BB) [19] was also run for one case. However, this model is generally no longer considered viable because it is ill-conditioned near the edge of boundary layers [20] (see also Appendix A).

The SA model is a one-equation model, solved for a variable related to the eddy viscosity. There are several versions with minor variations in use today. CFL3D employs the version referred to as SA-Ia. This is the version of the model that is given in Spalart and Allmaras [2]. OVERFLOW employs a modification to the SA-Ia model that is unpublished: it employs an additional term f_{v3} that multiplies part of the source term. From now on, this unpublished version will be referred to as SA, because most of the computations in the present study were run with it. The differences can be summarized as follows (refer to Spalart and Allmaras [2] for the form of the transport equation):

Version SA-Ia:

$$\hat{S} = \Omega + \frac{\hat{\nu} f_{v2}}{\kappa^2 d^2} \quad (1)$$

$$f_{v2} = 1 - \frac{\chi}{1 + \chi f_{v1}} \quad (2)$$

Version SA:

$$\hat{S} = f_{v3} \Omega + \frac{\hat{\nu} f_{v2}}{\kappa^2 d^2} \quad (3)$$

$$f_{v2} = \frac{1}{(1 + \chi/C_{v2})^3} \quad (4)$$

$$f_{v3} = \frac{(1 + \chi f_{v1})(1 - f_{v2})}{\chi} \quad (5)$$

The unpublished SA model tends to delay boundary-layer transition relative to the SA-Ia at moderately low Reynolds numbers (e.g., 1 to 10 million), even when the model is turned on everywhere (fully turbulent). At higher Reynolds numbers, the differences between the two versions are less significant.

The BB model is another one-equation model, that solves a field equation for a turbulence Reynolds number. The SST model is a two-equation model that solves equations for k and ω . Like SA, different versions of SST also exist in the literature (e.g., Menter [1] and Menter [21]). Both CFL3D and OVERFLOW employ the version from the latter reference. EASM is coded in CFL3D, but not in OVERFLOW. One significant difference between EASM and the other models used in this study is that EASM is a *nonlinear* model, for which nonlinear effects are included in the turbulent stresses. Like SST, EASM is a two-equation model. The form used in this study is a k - ω form [6].

The SA, SST, and EASM turbulence models have been used for validation on a wide variety of aerodynamic flows too numerous to mention here, for both 2-D and 3-D (see, for example, [7], [8], [22], [23], [24]). These validations include both attached and separated flows. In fact, one of the main features of these models that has caused their popularity and wide use throughout the world is their ability to do a better job predicting separated flows than other earlier models such as Baldwin-Lomax, Wilcox k - ω , and many of the “standard” forms of k - ε .

2.4 Description of Grids

A total of five grids were created for the current study. These are summarized in Table 1. In this table, OC signifies overspeed “cruise” condition, SS is small separation, BO is buffet onset, and BOF is buffet in flight. Each of the conditions OC, SS, and BO was defined from wind tunnel force data. The angles of attack determined from this methodology are: OC is $\alpha = 1.03^\circ$, SS is $\alpha = 1.5^\circ$, and BO is $\alpha = 2.8^\circ$.

The various wing model twist distributions (OC, SS, and BO) were measured in the wind tunnel with photogrammetry. Grid 1 uses the OC distribution, Grid 2 uses SS, and Grid 3 uses BO. The vertical displacements due to bending were estimated by scaling the model vertical displacements at cruise conditions relative to wind-off or zero-load conditions in a manner consistent with the ratio of measured twist increments. The flight vehicle is much more flexible than the scaled wind tunnel model. The wind tunnel model was designed to deform to the same shape as the flight vehicle when both are at cruise Mach number and flight Reynolds number; but at buffet, the flight vehicle has significantly larger deflections. As discussed in section 1.2, an *estimated* flight shape was obtained for the flight vehicle near buffet (BOF). This shape was obtained via flight-test-derived linear aerodynamics in a static loads analysis that used a 10,000 degree-of-freedom finite element model. This shape was used to determine the effect of large aeroelastic deformations on the results. Thus, Grid 4 is the wind tunnel model (without VGs or FSFs) deflected to the estimated shape of the flight vehicle at buffet.

All grids are overset grids with minimum normal spacing at walls such that the y^+ value is approximately 1, on average, for flow at a Reynolds number of 40 million. The far field extent of all grids is approximately 50 mean aerodynamic chords (MAC). Most grids contain over 7.1 million points. When every other point is removed from these, the resulting grids have approximately 890,000 points. A fine grid with nearly 22.6 million points was also generated (Grid 5). When every other point is removed, a coarser version of this grid contains approximately 2.8 million points.

As discussed earlier, the trailing edge of the wing (which has a small, but finite base thickness) is closed in all grids over one grid point. However, very near the wing tip (at and beyond a span station of 97.9%), closing the trailing edge rapidly in this manner caused problems in the grid generation, so this closure was relaxed in this region; instead, the grid was allowed to remain open for 8 additional points into the wake. Here, the grid was closed at a distance behind the trailing edge of roughly 3 - 4% of the local chord.

Some of the other characteristics of the grids are given here. The grids all use a C-mesh topology around the wing. The wing tip is closed off with a C-O-mesh type. Grids 1 through 4 (OC, SS, BO, and BOF) have 225 points streamwise on the wing (around in the C-mesh-direction) and 129 points spanwise. Grid 5 is refined primarily in the streamwise and normal directions: it has 449 points streamwise on the wing and about the same number of points spanwise as the other grids. All grids have tight clustering in the streamwise direction near the wing trailing edge: grids 1 through 4 have spacing of about 0.2% of the local chord, and Grid 5 has half of this. In all of the grids, the wake cut approximately bisects the trailing edge angle and “follows the wake” near the wing. Also, the grid lines parallel to the wing surface “open up” (spread) in the wake (i.e., the minimum normal spacing increases after the grid line passes aft of the trailing edge). This wake spreading is shown in a close-up view of the grid treatment near the trailing edge of the wing in Fig. 3. This view also shows the closure of the wake grid behind the trailing edge over one point.

The precise topology of each of the zones in the current grids is not described here. However, a few important general characteristics are as follows. Near the wing tip, a wing tip cap grid is employed. The engine nacelle and pylon use zones that wrap around their leading edges. The far field uses a Cartesian-like zone with some stretching. A view of a portion of the surface of Grid 3 is shown in Fig. 4. This figure gives an indication of the distribution of grid points on the wing. It also shows an overlap region, where the zone from the engine pylon overlaps a portion of the wing lower surface.

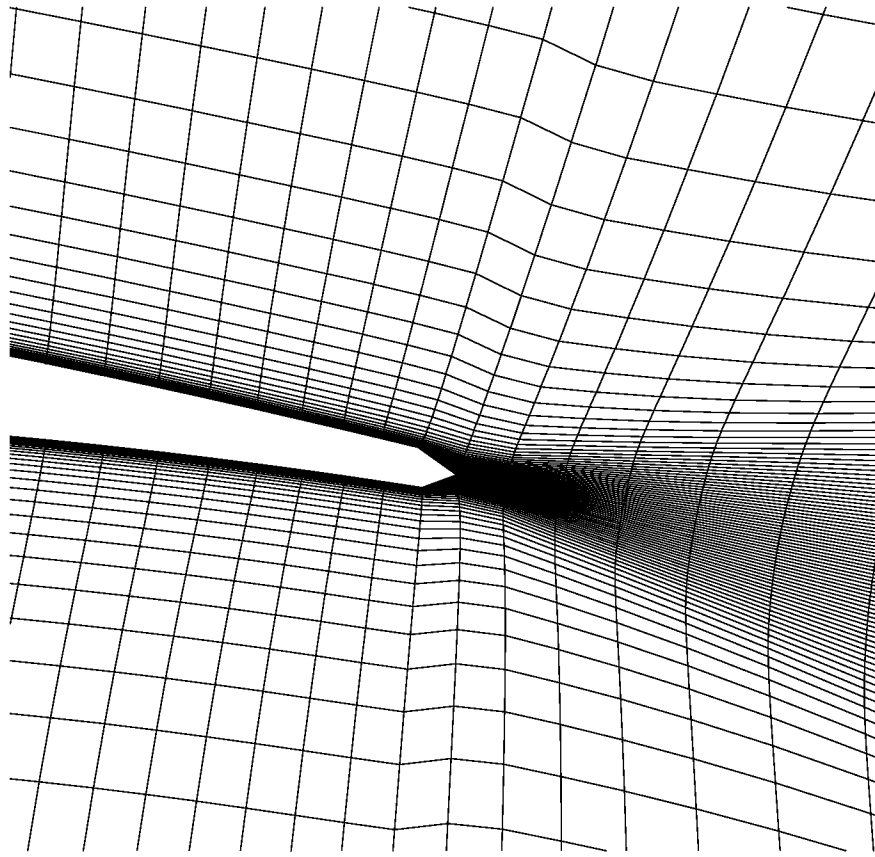


Figure 3: Close-up of a spanwise cut of the grid near the trailing edge of Grid 3.

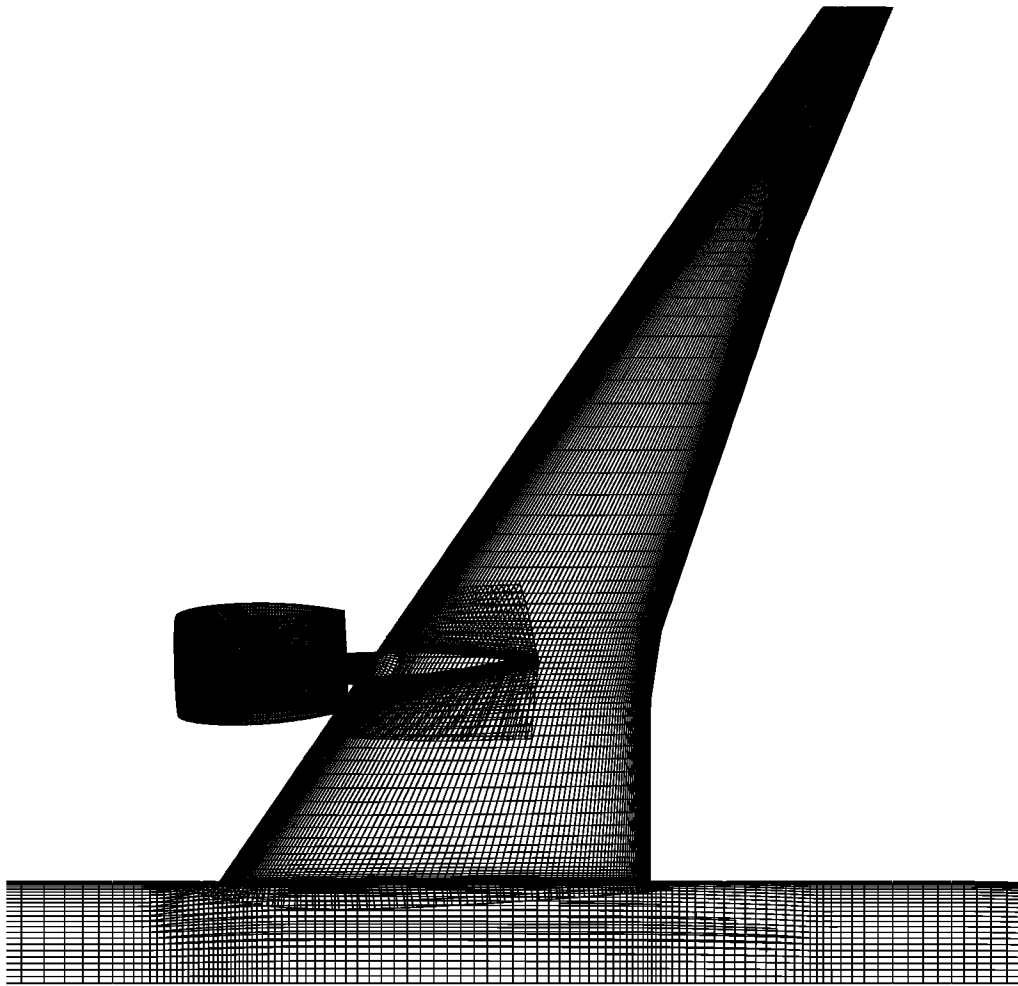


Figure 4: A portion of Grid 3, showing wing surface grid distribution.

The shape of the bifurcator (the small support bracket that holds the core cowl in place inside of the engine nacelle) was not defined in the geometry definition supplied to the grid generator; a bifurcator shape from a different aircraft configuration was used instead. Because the bifurcator only accounts for a relatively small amount of flow blockage, the use of a different shape is not expected to have a significant effect on the flow field. A head-on view of the computational model of the flow-through nacelle is shown in Fig. 5.



Figure 5: Head-on view of nacelle.

As discussed in section 2.1, the approach taken in the current study is to compute flow through the wind tunnel model’s “engine” by gridding the interior of the nacelle shown in Fig. 5. This avoids the need for additional boundary conditions at the engine inlet and exhaust faces. The mass flow through the nacelle can then be computed in terms of an equivalent free stream area, the stream tube of which passes through the nacelle. For the computations performed in this study, computed area values are approximately 3.7 - 5.1% high (depending on the case) compared to an estimated level based on the engine deck and airplane polars.

The current grids do not include horizontal or vertical tails; also, the sting is not included. The wind tunnel model was also run without a horizontal tail, but a thickened vertical tail is present in the form of a blade mount, and the sting extends back from the top of the vertical blade.

Finally, all grids are for half of the aircraft only. Symmetry boundary conditions are applied on the symmetry plane. The fuselage is computed as a viscous surface, and Riemann-type far

Table 1: Summary of overset grids generated

Grid	Wing twist	Number of grid points
1	OC (NTF model)	7,116,606
2	SS (NTF model)	7,116,606
3	BO (NTF model)	7,116,606
4	BOF (estimated flight vehicle)	7,116,606
5	BO (NTF model)	22,575,898

field boundary conditions are applied at all far field boundaries.

2.5 Summary of Computations Performed

A summary of the computations performed for the current study is given in Table 2. Most computations used OVERFLOW and the SA model, but there is a wide range of variation designed to systematically evaluate the effects of code, spatial differencing method, grid, turbulence model, and aeroelastic shape. All runs except runs 8 and 10 used upwind differencing. All runs were performed “fully turbulent” at $M = 0.87$ (the reason for this Mach number choice is discussed in section 1.2) and at a Reynolds number of 40 million based on MAC. A high Reynolds number was chosen to avoid questions regarding transition location, and because it is representative of the flight Reynolds number. NTF runs were conducted at $Re = 40$ million (as well as at lower Reynolds numbers down to that attainable in conventional wind tunnels).

Each case run using CFL3D or OVERFLOW was considered to be converged when the drag coefficient variation with additional multigrid cycles dropped to less than one drag count (0.0001). At the higher angles of attack (above 4°), however, some of the computations exhibited small levels of oscillatory behavior (e.g., oscillation in drag coefficient of on the order of 2 drag counts), usually indicating a tendency for unsteadiness in the computed flow. In these cases, time-accurate runs were not pursued; rather, representative force values were chosen from the non-time-accurate runs.

Actual numerical values of the computed forces and moments for each of the runs are not given in this paper. However, detailed comparisons using figures without axis labels will be given in sections 3, 4, and 5.

2.6 Summary of Current “Best Practices”

This section contains a summary of “best practices” for applying CFD to an aerospace configuration such as the current aircraft. These guidelines arose from a group consensus of the experienced CFD practitioners in this study, and were followed in the present work.

1. Approximate the physical model (geometry) as closely as possible in the CFD grid. If walls, brackets, supports, etc. are ignored, recognize the fact and have a good idea of the effects that might be missed.
2. Be aware of the aeroelastic deformations of the model or flight vehicle, and account for these in the CFD grid or be aware of their effects.

Table 2: Summary of computations performed at $M = 0.87$, $Re = 40$ million

Run	Condition	Grid	α , deg.	Code	Turbulence model
1	OC	1	1.03	OVERFLOW	SA
2	OC	1	0.8979	OVERFLOW	SA
3	BO	1	2.8	OVERFLOW	SA
4	SS	2	1.5	OVERFLOW	SA
5	BO	3	2.8	OVERFLOW	SA
6	BO	3 (coarsened)	2.8	OVERFLOW	SA
7	BO	3	2.8	OVERFLOW	SST
8	BO	3	2.8	OVERFLOW (central)	BB
9	BO	3 (closer FF)	2.8	OVERFLOW	SA
10	BO	3	2.8	OVERFLOW (central)	SA
11	BO+	3	3.0	OVERFLOW	SA
12	BO-	3	2.5	OVERFLOW	SA
13	BO	3	2.8	OVERFLOW	SA-Ia
14	BO	3	2.8	CFL3D	SA-Ia
15	BO	3	2.8	CFL3D	SST
16	BO	3	2.8	CFL3D	EASM
17	BO	4	2.8	OVERFLOW	SA
18	BO	5	2.8	OVERFLOW	SA
19	BO	5 (coarsened)	2.8	OVERFLOW	SA
20	past BO	3	4.0	OVERFLOW	SA
21	past BO	3	5.1	OVERFLOW	SA
22	past BO	4	4.0	OVERFLOW	SA
23	past BO	4	5.1	OVERFLOW	SA
24	past BO	4	7.0	OVERFLOW	SA
25	past BO	4	9.0	OVERFLOW	SA
26	SS	2	1.5	CFL3D	EASM
27	past BO	3	4.0	CFL3D	EASM

3. Use a sufficient grid resolution and perform a grid sensitivity study to estimate discretization errors.
4. Use correct boundary conditions. If the case is a wind tunnel comparison, investigate the effect of wind tunnel walls. If it is a free-air computation, ensure that the far field boundary condition is applied sufficiently far away.
5. Maintain grid smoothness (quality) in structured grids as much as possible: maintain reasonable orthogonality, avoid too-large stretching factors and too-rapid turnings or twistings of grid face normal directions.
6. Do not leave a gap in the wake cut behind a blunt trailing edge, particularly for attached flows.
7. Cluster grid lines near the wing trailing edge in the streamwise direction to be less than or equal to approximately 0.2% of the local chord. Cluster grid lines near wing leading edge in the wrap-around direction to be less than or equal to approximately 0.1% of the local chord.
8. Set the minimum spacing at walls to be small enough such that the y^+ levels are near 1 or less for turbulent flows.
9. When computing turbulent flows, always verify the resulting computed transition location by looking at eddy viscosity contours or some other appropriate measure. Running “fully turbulent” does *not* guarantee transition to turbulence at the leading edge; the actual trip location is a function of the turbulence model and the Reynolds number.
10. Spread grid lines in the wing wake (but not too rapidly); approximately follow the trailing edge bisector angle to try to align the grid lines with the local flow direction.
11. Using more than one CFD code for a given case can help lend confidence to the validity of the results and also give an idea of the magnitude of differences due to different numerical treatments; however, be aware of differences in the *turbulence model equations* employed (i.e., be aware of turbulence model versions and implementation differences used by different codes).
12. Determine the pedigree of experimental and flight data. Corrections are often applied to the data that limit its usefulness in direct comparison to CFD results. Do not trust experimental data blindly.

3 CFD SENSITIVITY ANALYSIS

All the results for the CFD sensitivity analysis are for the buffet onset (BO) condition ($\alpha = 2.8^\circ$). This case has a significant amount of separated flow on the wing, as shown in a plot of wing upper surface streamlines in Fig. 6 (run 5). Mach contours at four spanwise stations on the wing are shown in addition to the surface streamlines in Fig. 7. This second figure gives an indication of the relative position of the shock wave in space, as well as an indication of the off-surface extent of separated flow behind the shock.

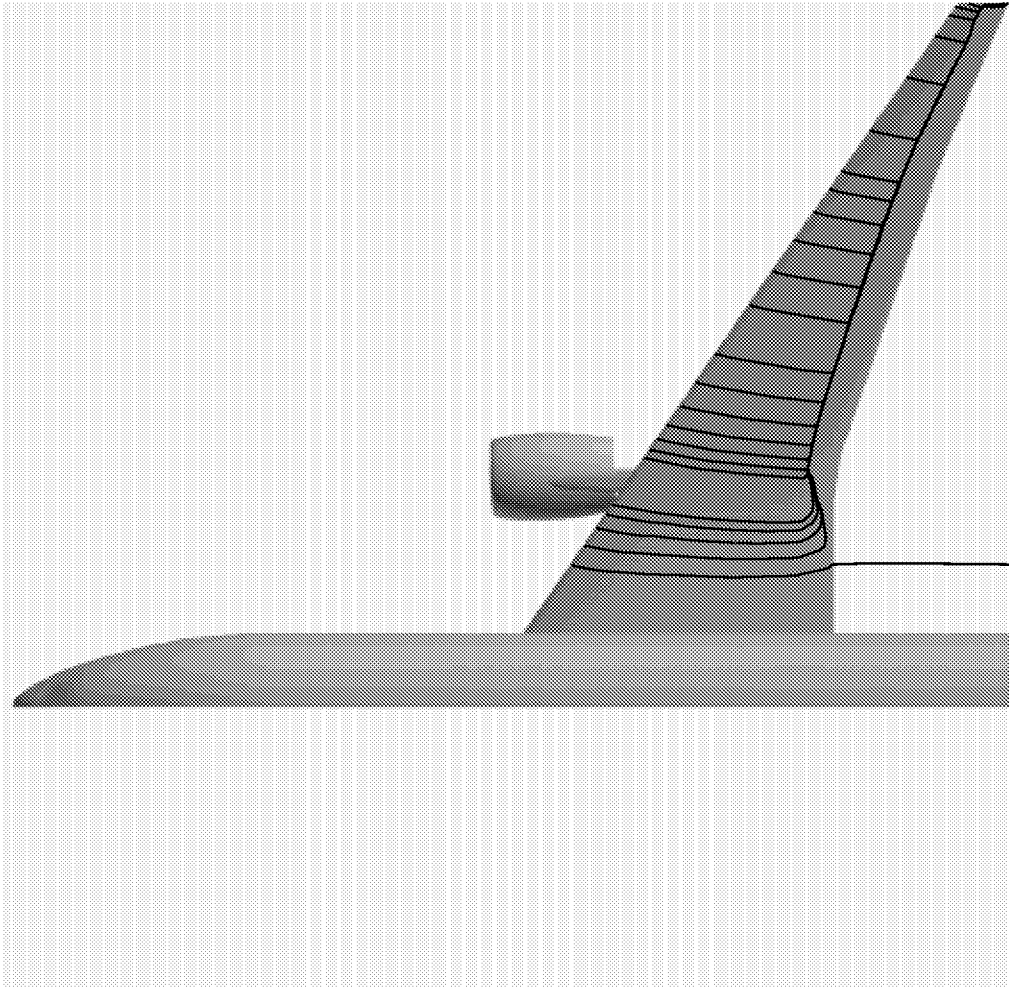


Figure 6: Wing upper surface streamlines at BO condition, OVERFLOW, SA model.

3.1 Effect of Grid

The effect of grid density on the surface pressure coefficients of the buffet onset case is shown in Fig. 8. In this and all subsequent plots of surface pressure coefficients to follow, only the C_p levels on the upper surface are shown, for company proprietary reasons. Shown are results from runs 18, 5, and 19 (on Grid 5, Grid 3, and on every other grid point from Grid 5). Results using the coarsened Grid 3 (run 6) are not shown in this figure. Globally, results appear to be

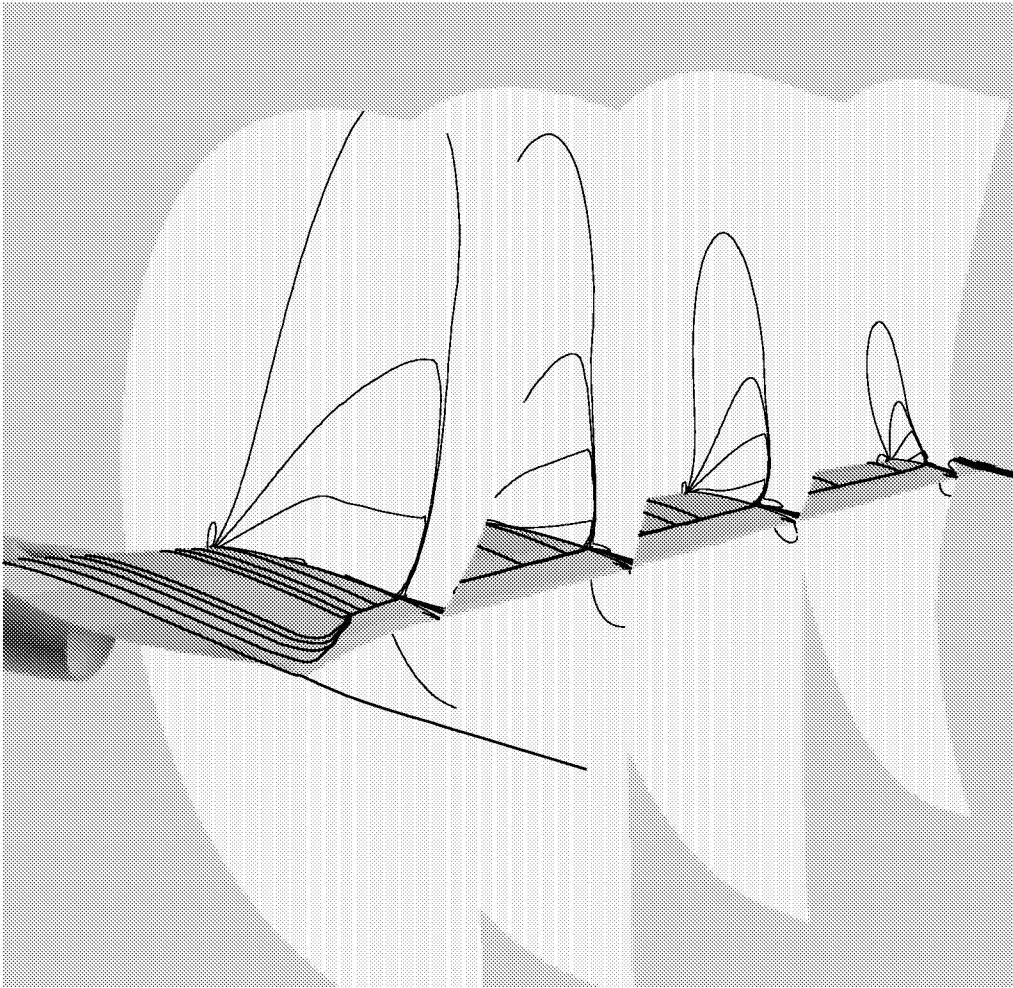


Figure 7: Mach contours at four span stations (approximately $2y/B = 0.4, 0.6, 0.8,$ and 0.95) along with wing upper surface streamlines at BO condition, OVERFLOW, SA model.

reasonably well grid-converged even on the grid with 2.8 million points, although the pressure levels in the separated regions behind the shock at the outboard-most stations show a small shift on the finest grid. This shift probably indicates that the separated region on the outer quarter of the wing is not adequately resolved on the two coarser grids. However, the shock position remains unchanged on all three grids.

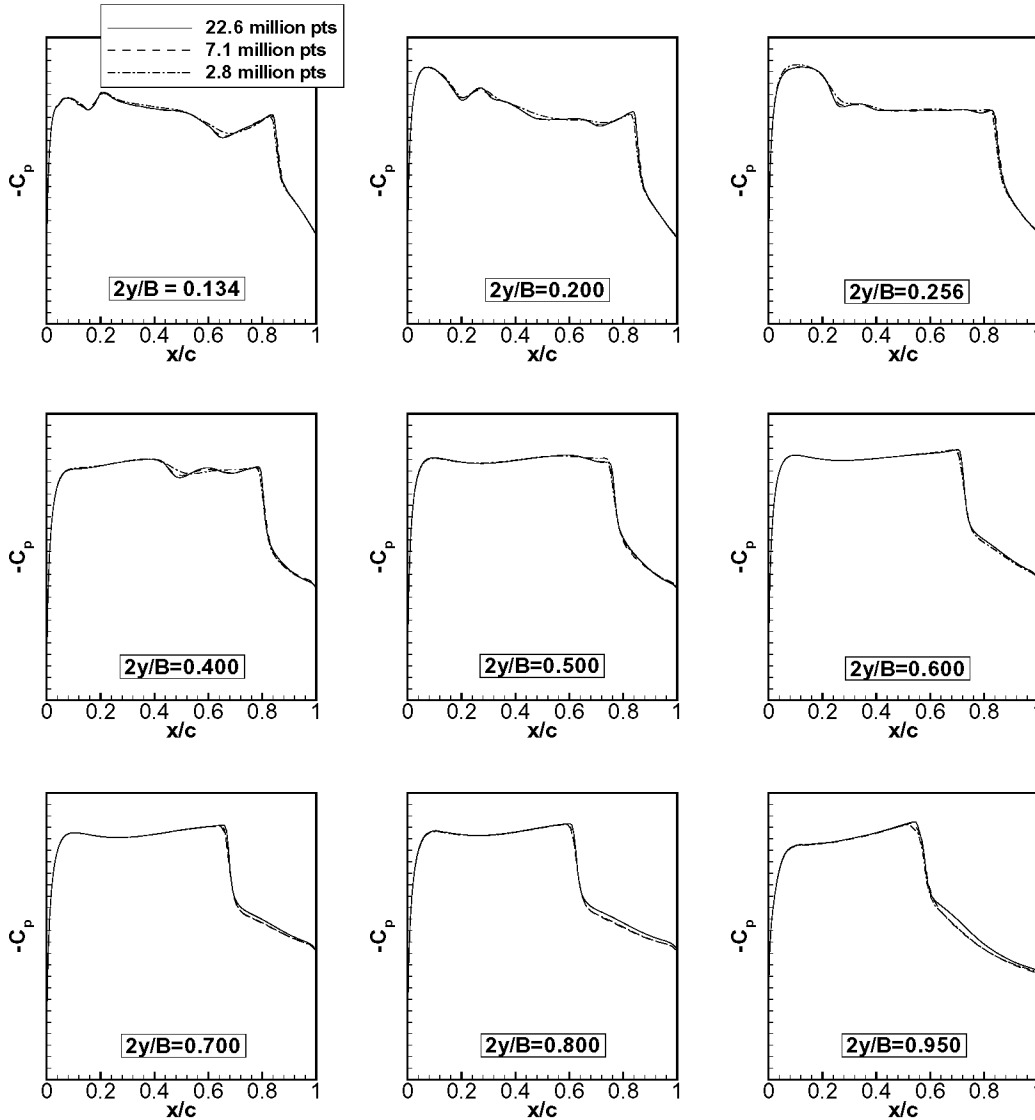


Figure 8: Effect of grid density on surface pressure coefficients, OVERFLOW, SA model.

Although not shown here, lift coefficient, drag coefficient, and pitching moment coefficient about the quarter-chord MAC location can be plotted as a function of $N^{-2/3}$, where N is the total number of grid points. For a 3-D scheme that is globally second-order accurate in space, plotting against this variable should yield a linear variation on sufficiently fine grids, for a given structured-grid family. (A family consists of grids with the same distribution functions and relative grid index relationships. For example, when a second grid is created by taking every other point from a finer grid, then the two are in the same family.) Due to computational constraints,

Table 3: Force and moment error on each grid, for BO condition

Grid	Number of grid points	% Lift error	% Drag error	% Moment error
5	22,575,898	0.09	0.66	0.18
3	7,116,606	0.61	1.40	2.82
5 (coarsened)	2,821,987	0.73	2.62	2.87
3 (coarsened)	889,576	2.40	7.75	4.90

the finest grid (22.6 million points) is not double the grid density in each index direction from the grid with 7.1 million points, so the two are *not* in the same family. Nonetheless, a linear variation was assumed to exist using the three finest grids, and results on an infinite density grid were inferred using a least-squares fit to the data.

Using the inferred results on an infinite density grid, the percent error can be computed for each of the finite grid sizes. These results are tabulated in Table 3. Grid 3, which is the default grid size for all the remaining computations in this paper, is in error from an infinitely refined grid by less than 1% in lift, less than 2% in drag, and less than 3% in moment for the buffet onset case.

Run 9 was performed to assess the adequacy of the default far field extent of approximately 50 MAC. Results using an extent of 25 MAC are indistinguishable from the 50 MAC results, so pressure coefficients are not shown here. Quantitatively, the lift and drag on the grid with closer far field are both lower by approximately 0.1%, and the moment is lower by only 0.01%. This comparison indicates that the far field extent of 50 MAC is sufficiently far to yield forces and moment with accuracy below 0.1%.

3.2 Effect of Code and Spatial Differencing Method

Recall from section 2.3 that OVERFLOW and CFL3D have different implementations of the SA turbulence model. Most runs with OVERFLOW in this study use the unpublished version (SA). However, the effect of the different versions was investigated by coding SA-Ia into OVERFLOW, and comparing results between SA and SA-Ia for OVERFLOW alone (runs 5 and 13). Although not shown, results using the two turbulence model versions are almost identical: the lift, drag, and moment are different by less than 0.02%. (The Reynolds number of 40 million is high enough such that both turbulence model versions transition immediately at the wing leading edge.)

The effect of running the two different codes for the buffet onset case using the same grid and same turbulence model (SA-Ia) is shown in Fig. 9 (runs 13 and 14). The comparison shows that results are very similar between OVERFLOW and CFL3D in general, with the largest differences at the outboard stations downstream of the shock. Lift is predicted to be approximately 2% higher, drag is 2% higher, and moment is 6% lower for CFL3D.

The effect of spatial differencing of the convective terms was also investigated. OVERFLOW was run both with upwind differencing as well as with central differencing (all other OVERFLOW runs in this study use upwind differencing). Results from runs 5 and 10 are plotted in Fig. 10. There is only a small difference between results. The central difference method tends to yield a more smeared-out shock, as expected. The lift from the central difference run is 0.8%

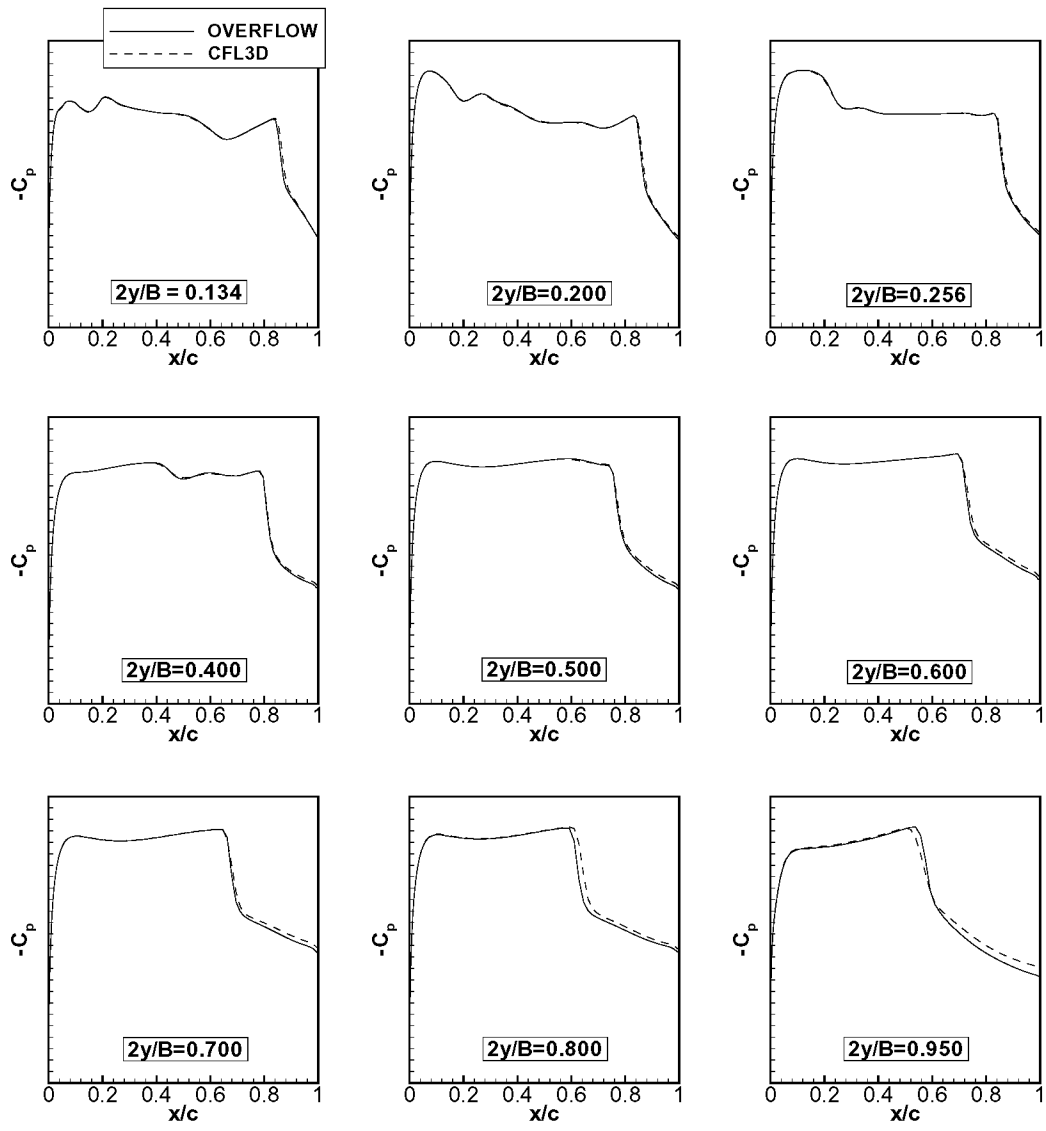


Figure 9: Effect of code on surface pressure coefficients, SA-Ia model.

lower, the drag 0.07% higher, and the moment 0.6% lower than the upwind result.

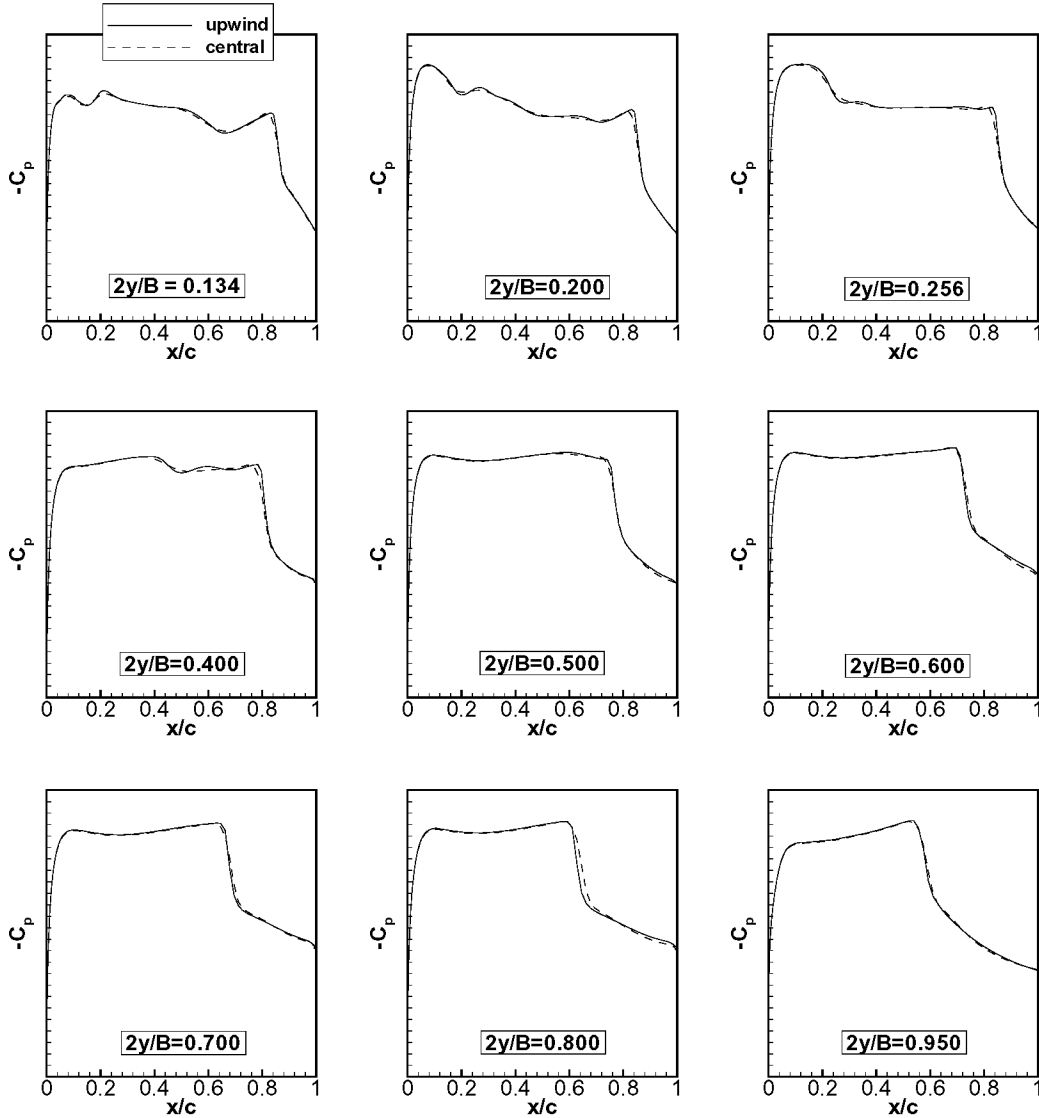


Figure 10: Effect of spatial differencing on surface pressure coefficients, OVERFLOW, SA model.

3.3 Effect of Aeroelastic Shape

Aeroelastic wing deformation can be significant for an aircraft, whereas for wind tunnel models in the NTF it is less of a factor (although not negligible). Fig. 11 shows the percent change in twist of the wind tunnel model's wing and the flight vehicle's wing at 95% span station between the respective 1-g condition and the buffet onset condition. Photogrammetry was used to obtain the twist change for the wind tunnel model, and a finite element model was used for the aircraft. The figure indicates the relatively large change in twist of the flight vehicle relative to the wind tunnel model. The wind tunnel model is designed so that at the 1-g condition (at

cruise Mach number and flight Reynolds number), its twist matches the twist of the aircraft wing at the same conditions. Clearly, therefore, at off-design conditions the two wing shapes will not match because of their different flexibility characteristics.

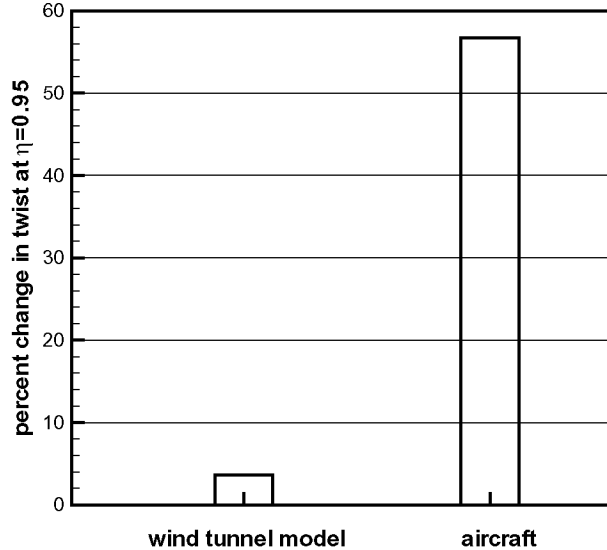


Figure 11: Change in twist between respective 1-g condition and buffet onset condition at $\eta = 0.95$ for two wings.

The effect of aeroelastic shape on the buffet onset case was investigated with runs 3, 5, and 17. Results are plotted in Fig. 12. Recall that Grid 1 represents the shape of the NTF model wing at the overspeed “cruise” condition (OC) of $\alpha = 1.03^\circ$, Grid 3 is its shape for buffet onset (BO) at $\alpha = 2.8^\circ$, and Grid 4 is an estimated shape based on the flight vehicle at its buffet onset (BOF).

Each of runs 3, 5, and 17 uses an angle of attack of $\alpha = 2.8^\circ$, so the results using Grid 3 are expected to be the most representative of the NTF model at this condition. But because the NTF model is comparatively stiff, the aeroelastic shape change is fairly small between Grid 1 and Grid 3, and results are very similar. The difference is 0.7% in lift, 2.4% in drag, and 0.7% in moment. Grid 4, representative of the *flight* vehicle’s elasticity, has much greater deflection and twist. Results using Grid 4 are significantly different from the others outboard of mid-span. For example, the shock location is further downstream at the outboard span stations. The difference between results using Grid 4 and Grid 3 are 4% in lift, 11% in drag, and 6% in moment.

It should be stressed here that this is not a straightforward comparison. Buffet onset in the wind tunnel model occurs at $\alpha = 2.8^\circ$. However, when the flight vehicle wing shape for buffet onset at $M = 0.87$ was estimated, conditions at the buffet lift coefficient were used, which correspond to an approximate angle of attack of $\alpha = 5.1^\circ$. Moreover, the specific process used to determine the angle of attack at buffet is not straightforward, but rather relies on some heuristic methodology. There is also some uncertainty in angle of attack due to aircraft fuselage aeroelastics. So results using the estimated BOF shape should be assessed with caution; it is

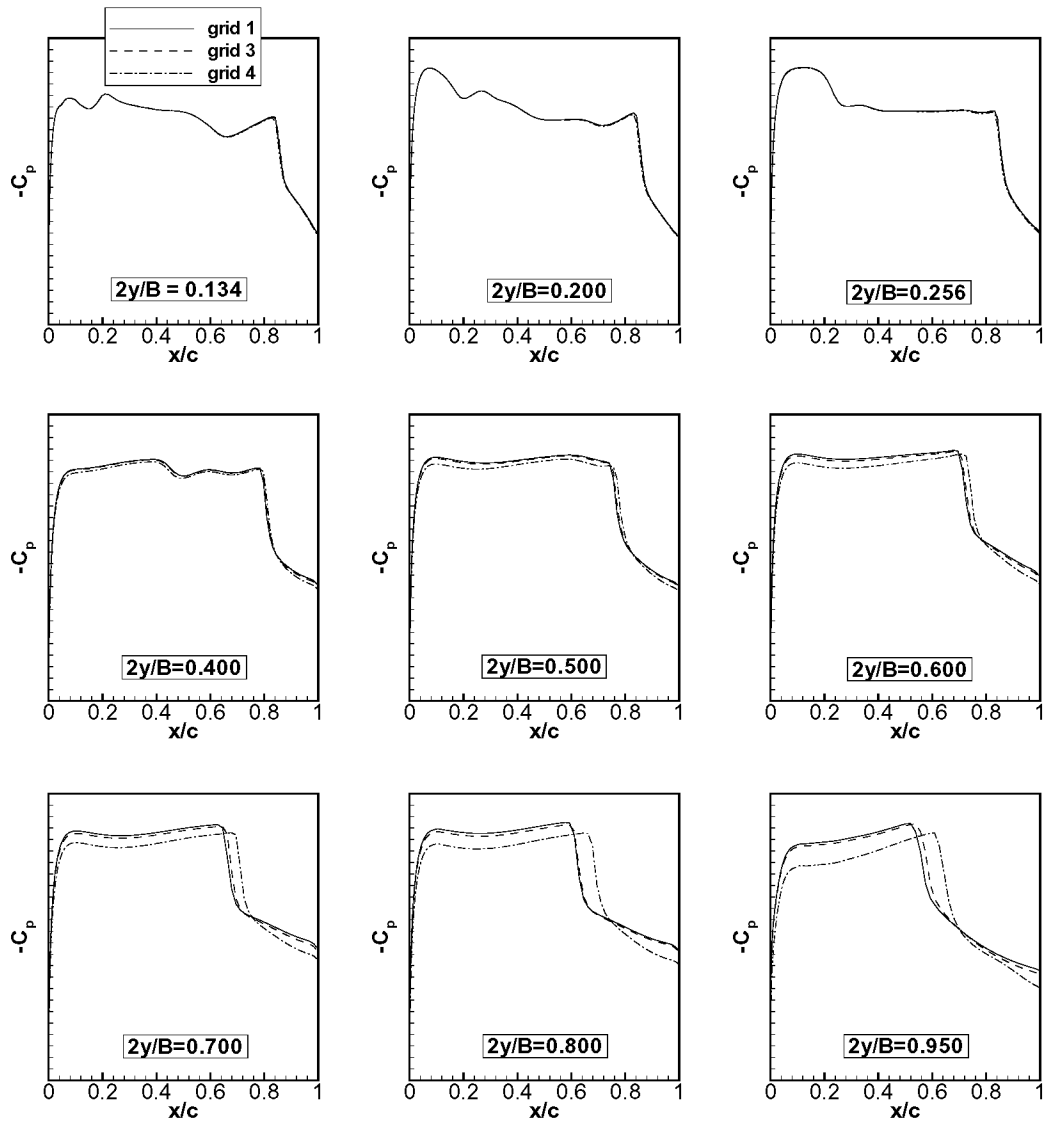


Figure 12: Effect of aeroelastic shape on surface pressure coefficients, OVERFLOW, SA model (grid 1 = OC NTF model, grid 3 = BO NTF model, grid 4 = BOF estimated flight vehicle).

not entirely clear what the shape actually represents. For now, we use it only to obtain a rough idea of the magnitudes of the *possible* effects due to aeroelastic differences between the wind tunnel model and the flight vehicle.

3.4 Effect of Turbulence Model

The effect of three different turbulence models using CFL3D is shown in Fig. 13, using runs 14, 15, and 16. Results show only relatively small differences in the predicted results. The SST model tends to yield the farthest-forward shock location, and EASM the farthest aft. The difference is most pronounced at the last span station near the wing tip. The maximum difference in lift between these three cases is 3.1%, maximum difference in drag is 4.4%, and maximum difference in moment is 8.3%.

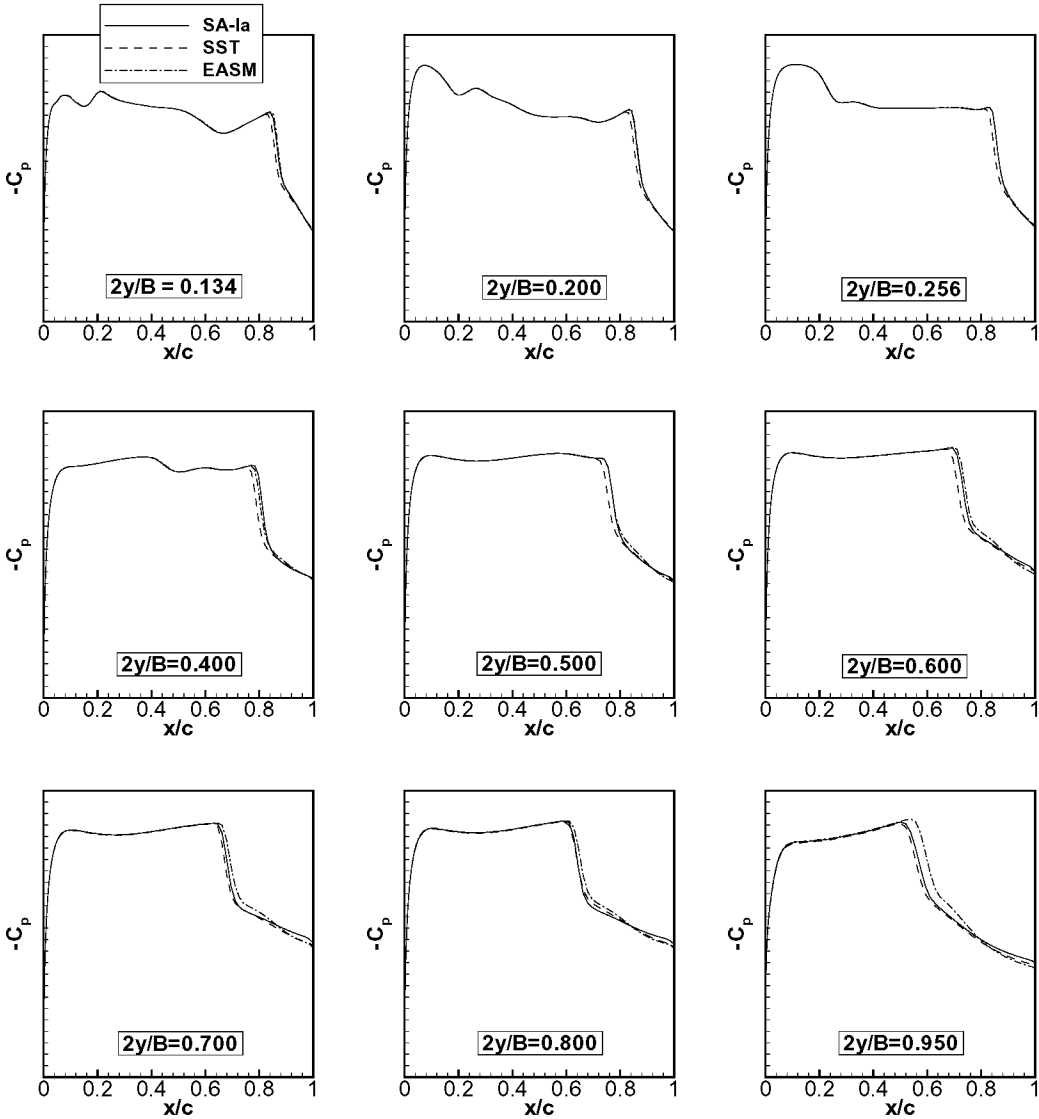


Figure 13: Effect of turbulence model on surface pressure coefficients, CFL3D.

The effect of three different turbulence models using OVERFLOW is shown in Fig. 14, using runs 5, 7, and 8. Note that the BB model used central differencing, whereas the other two models used upwind differencing. However, based on results in section 3.2, the differences due to spatial differencing on the grid with 7.1 million points is probably very small. The three turbulence models predict very similar results. Again, SST tends to predict the shock farthest forward, but of these three turbulence models, SA tends to predict the shock farthest aft. The maximum difference in lift between these three cases is 2.9%, maximum difference in drag is 4.3%, and maximum difference in moment is 6.2%.

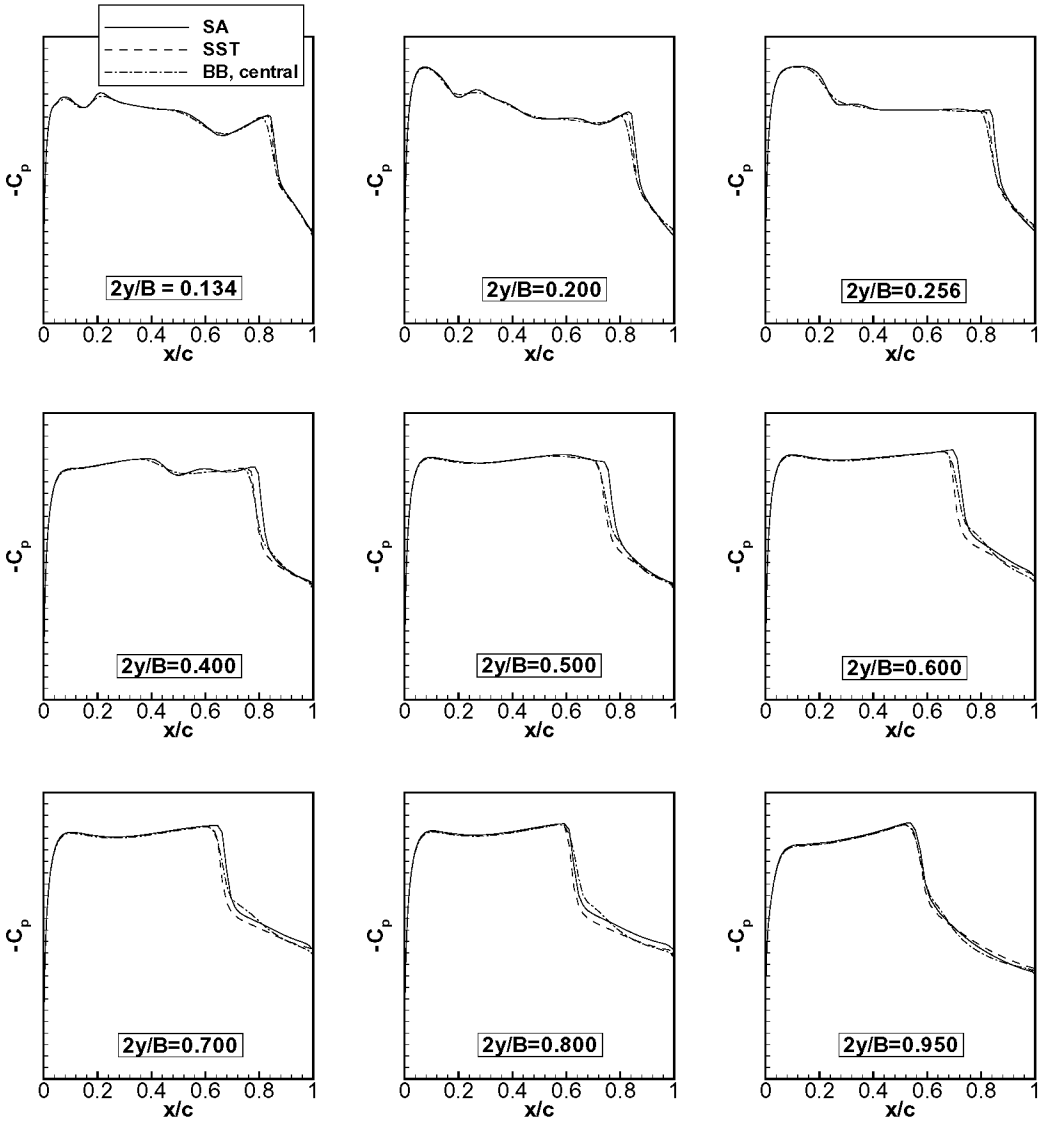


Figure 14: Effect of turbulence model on surface pressure coefficients, OVERFLOW.

3.5 Summary of CFD Sensitivities

This section summarizes most of the differences presented so far, in terms of the forces and moments. In the following, we show only results on grids 1 and 3 (each with 7.1 million points). Grid density effects were established earlier in section 3.1 and are not repeated here. Because grid 4 does not correspond with a wind tunnel model aeroelastic shape, we leave it out of this summary.

Lift coefficients are shown in Fig. 15. In the figure, “O” indicates OVERFLOW and “C” indicates CFL3D. The left-most bar labeled with “1-g” indicates the use of Grid 1 (the wind tunnel model shape for the 1-g OC case, run 1). All the other results in the figure use Grid 3. “Central” indicates central differencing (as opposed to upwind differencing), and “closer” indicates results using the grid with closer far field extent. The solid horizontal line indicates the mean of the ten results, and the dashed lines denote the range for the mean plus or minus 1σ , where σ is the standard deviation. Results for drag and pitching moment are given in Figs. 16 and 17, respectively. Most of the results in the three figures lie within $\pm 1\sigma$ (denoted in the figures) of the mean. In general, the choice of turbulence model and code have the most significant effect on the predictions, with CFL3D tending to give larger forces and (negative) moments than OVERFLOW for a given turbulence model.

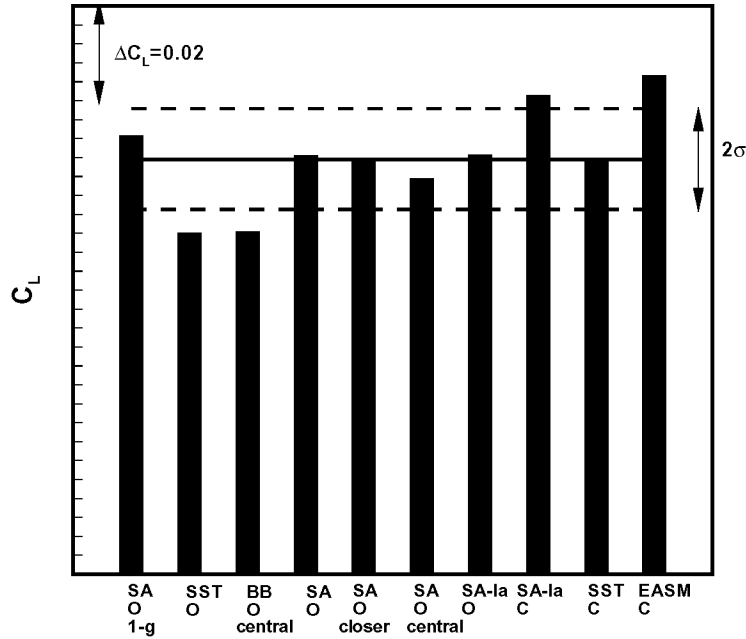


Figure 15: Summary of the predicted lift coefficients for the BO condition.

A summary plot is given in Fig. 18 showing the maximum variation in lift, drag, and pitching moment for the four categories of grid size, code/differencing, tunnel model aeroelastics, and turbulence model. The grid error represents the error from using a grid with 7.1 million points compared to interpolated results using a grid of infinite density for this case.

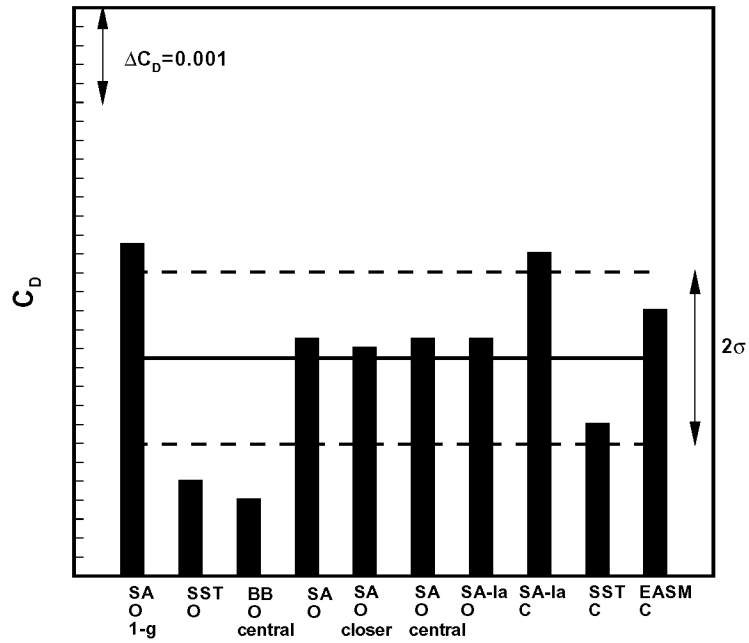


Figure 16: Summary of the predicted drag coefficients for the BO condition.

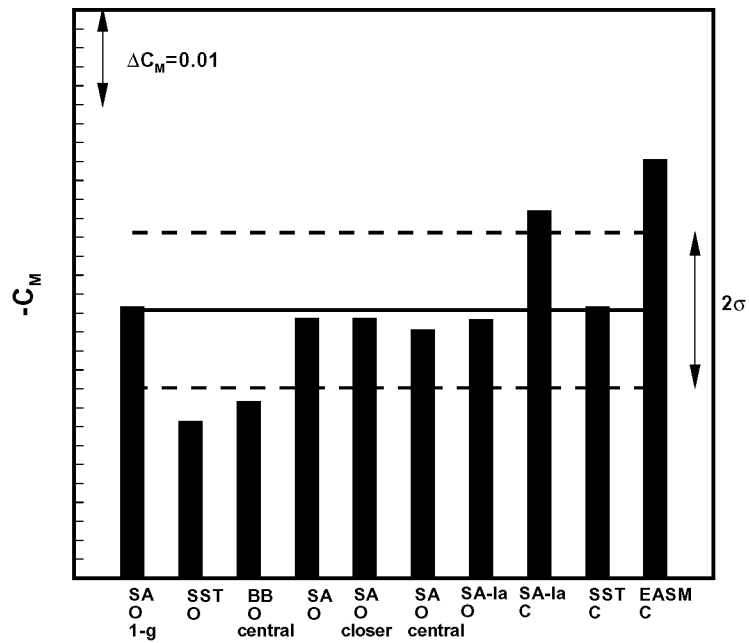


Figure 17: Summary of the predicted moment coefficients for the BO condition.

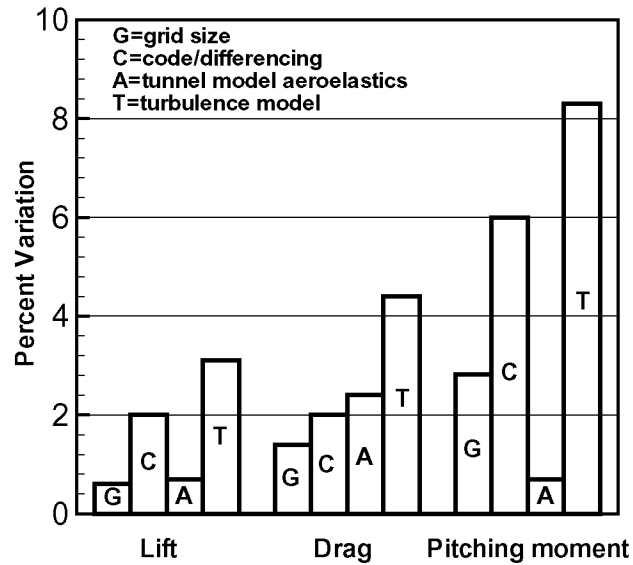


Figure 18: Established CFD variations for the BO condition, using grid with 7.1 million points.

In summary, for this modern civil transport buffet onset case, we have established an “error band” for the CFD, applying a consistent set of best practices. Given a grid of sufficient density (e.g., 7.1 million points for this case) for a given aeroelastic wing shape, the combined approximate maximum variation of computed forces and moments due to individual differences in code, spatial differencing method, and turbulence model are: 6% in lift, 7% in drag, and 16% in pitching moment.

This result presupposes that one of only four turbulence models – SA, SST, BB, or EASM – is used. As mentioned in the introduction, these models tend to perform better for separated flows than many other models. If one was to use the Baldwin-Lomax model for this case, for example, one would likely see much larger variations.

4 COMPARISONS WITH WIND TUNNEL DATA

At $M = 0.87$, the overspeed “cruise” (OC) condition corresponds to an angle of attack of $\alpha = 1.03^\circ$. At this angle of attack, the flow over the upper surface is mostly attached, with a small amount of flow turning near the trailing edge, as seen in the upper surface streamlines in Fig. 19 (run 1). Mach contours at four span stations are superimposed on the streamline plot in Fig. 20. Results computed with OVERFLOW and the SA model (run 1 in Table 2) are compared with wind tunnel data in Fig. 21. Note that the angle of attack of the wind tunnel model in this case is $\alpha = 1.1^\circ$, which is the closest wind tunnel condition to the OC angle of attack of $\alpha = 1.03^\circ$. Overall, results agree very well with experiment. Often, users of CFD in industry run CFD codes to match the lift when comparing against experimental pressures near design conditions. This was also done for the current case: OVERFLOW was run to approximately match the wind tunnel lift level (run 2). These results are also plotted in the figure. The “fixed C_L ” option has only a very small effect, mostly on the upper surface near the leading edge.

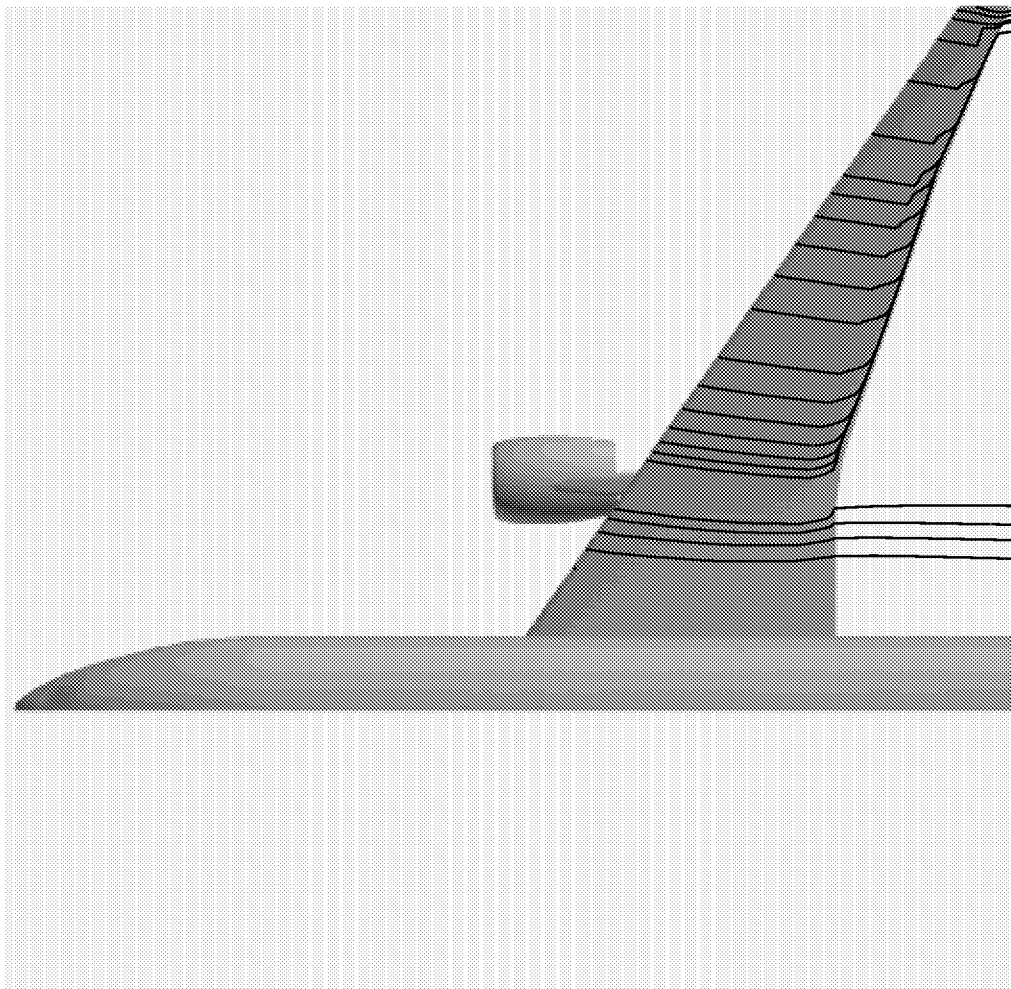


Figure 19: Wing upper surface streamlines at OC condition, OVERFLOW, SA model.

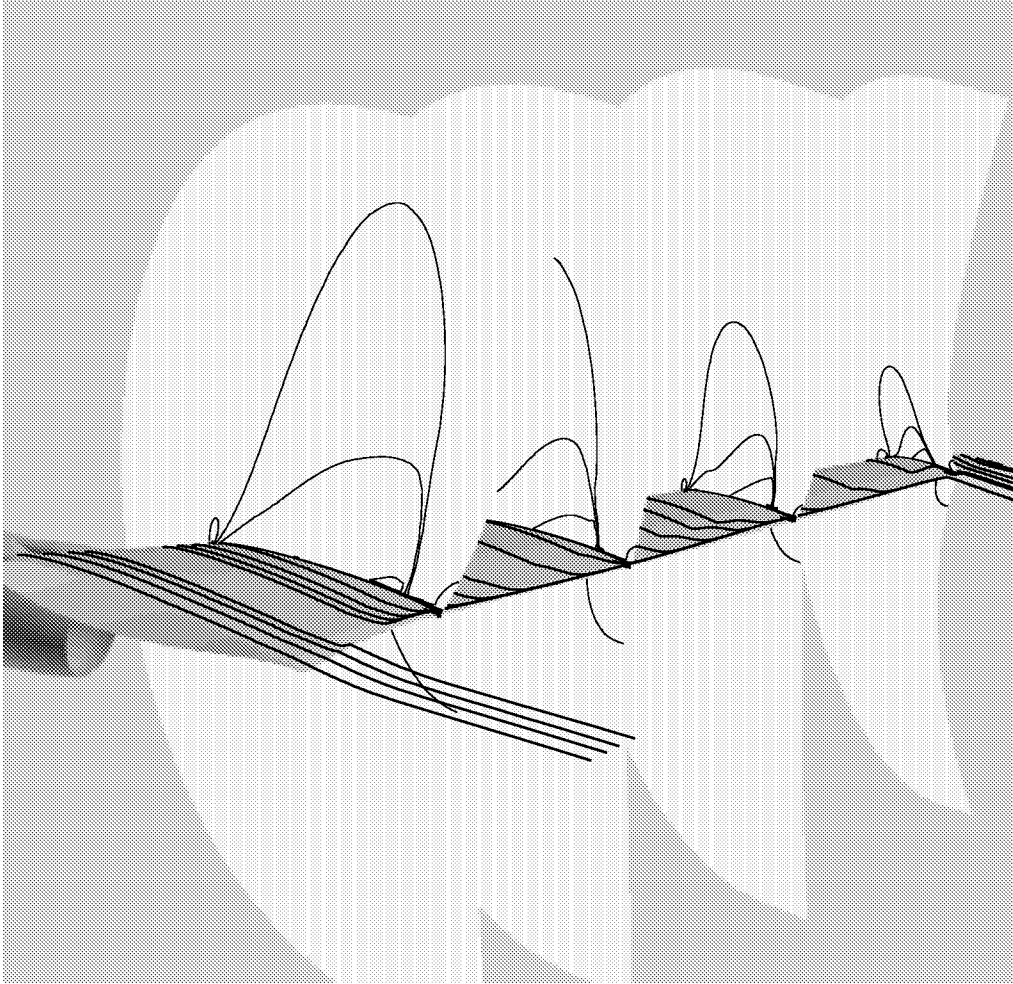


Figure 20: Mach contours at four span stations (approximately $2y/B = 0.4, 0.6, 0.8,$ and 0.95) along with wing upper surface streamlines at OC condition, OVERFLOW, SA model.

The small separation (SS) case corresponds to $\alpha = 1.5^\circ$. At this angle of attack, the flow over the upper surface exhibits a small amount of separation near the wing trailing edge, as seen in the upper surface streamlines in Fig. 22 (run 4). Mach contours are given in Fig. 23, and the surface pressure coefficients are plotted in Fig. 24 (wind tunnel model angle of attack in this case is $\alpha = 1.6^\circ$). CFD results are again in very good agreement with wind tunnel data, although the CFD predicts the shock slightly too far aft at the $2y/B = 0.80$ station.

Surface streamlines and Mach contours for the buffet onset case were shown previously in Figs. 6 and 7 (run 5). Although not shown, different turbulence models applied to the BO case yield surface streamlines and Mach contours that are almost indistinguishable from those obtained using SA. The surface pressure coefficients are plotted in Fig. 25 (wind tunnel model angle of attack in this case is $\alpha = 2.9^\circ$). Overall, agreement is good at inboard stations, but the CFD predicts the shock too far aft beginning at mid-span and extending out to the $2y/B = 0.80$ station. Agreement is good again at the station nearest the wing tip.

Fig. 26 shows the progression of the shock forward as the angle of attack is increased from

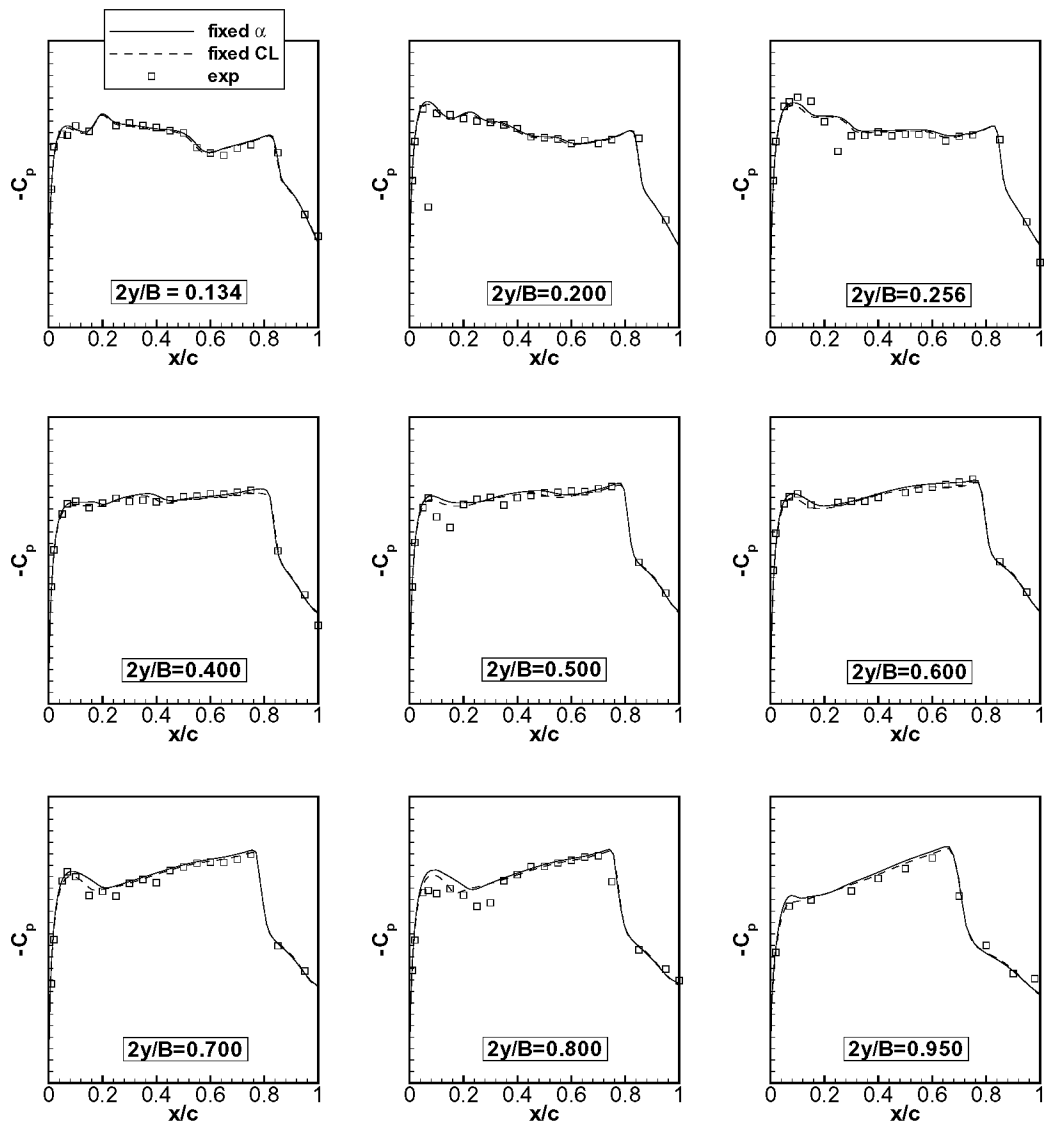


Figure 21: Predicted surface pressure coefficients at OC condition, OVERFLOW, SA model.

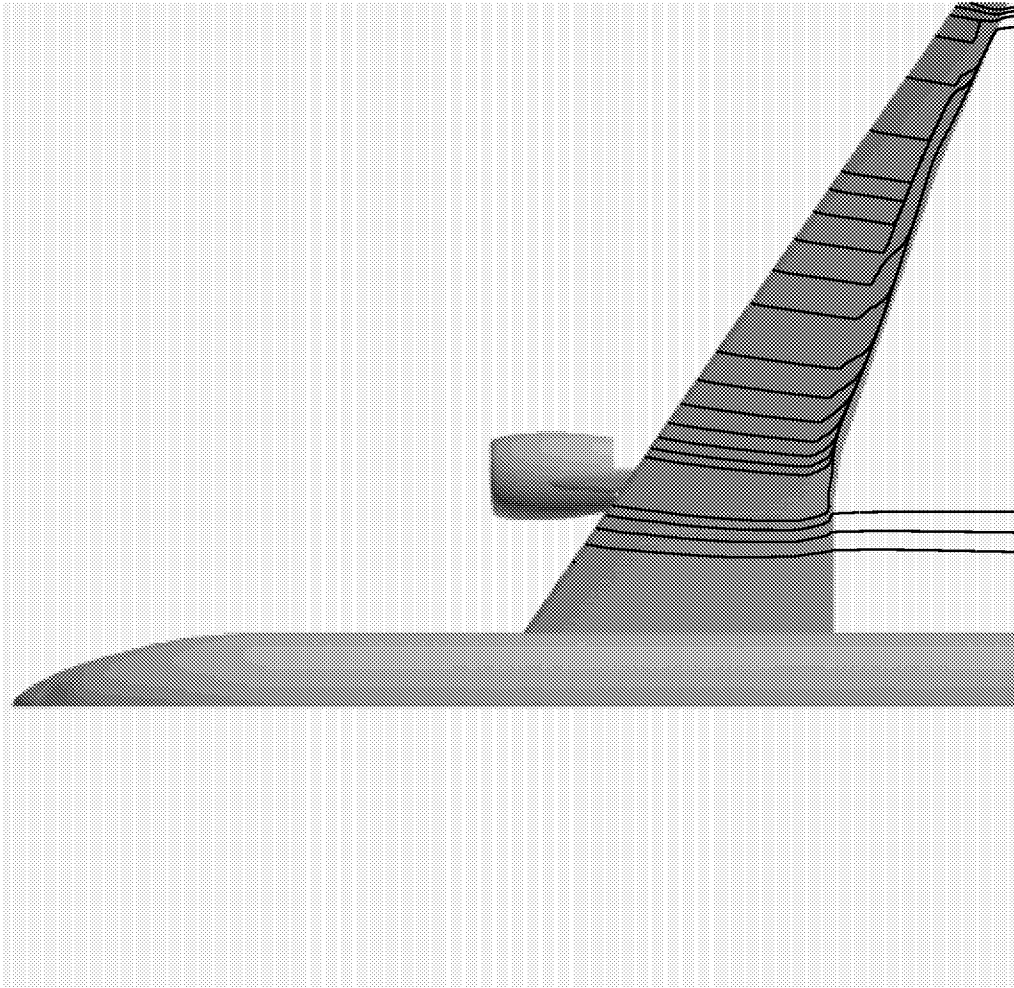


Figure 22: Wing upper surface streamlines at SS condition, OVERFLOW, SA model.

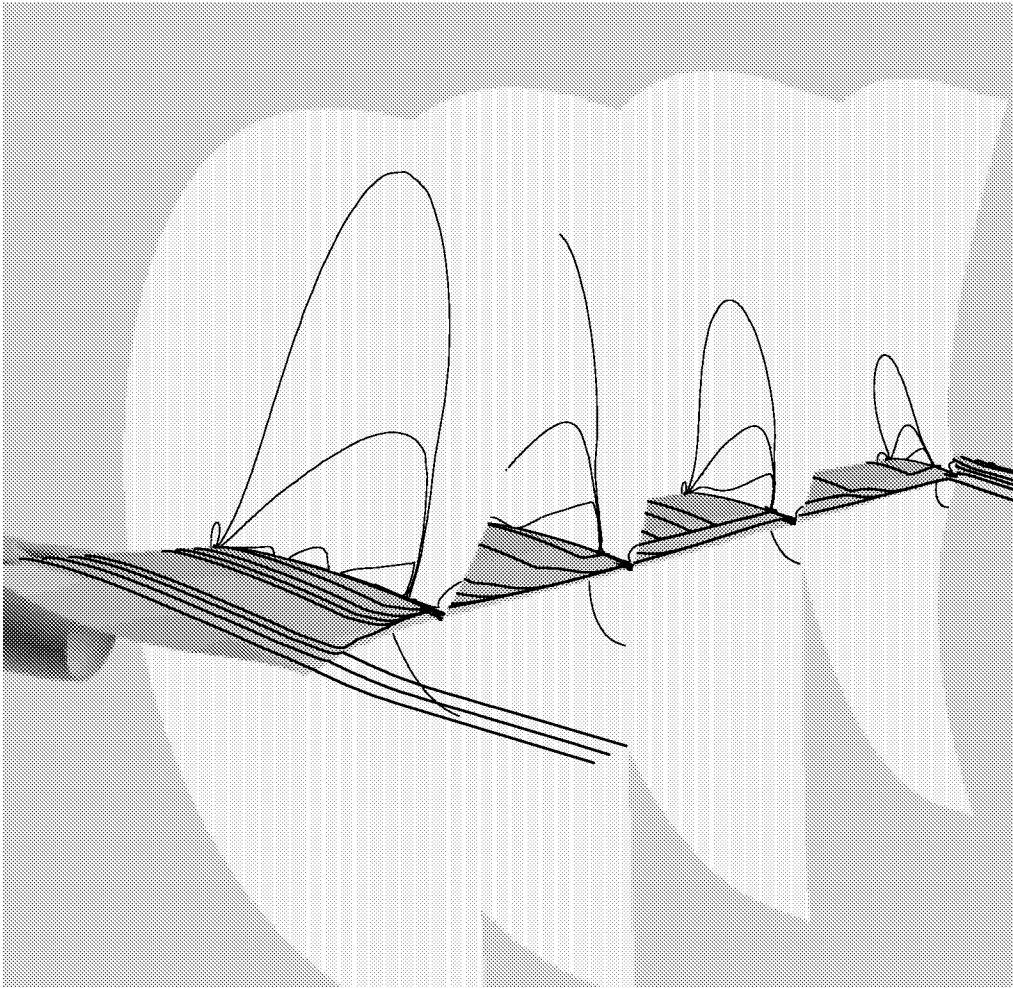


Figure 23: Mach contours at four span stations (approximately $2y/B = 0.4, 0.6, 0.8,$ and 0.95) along with wing upper surface streamlines at SS condition, OVERFLOW, SA model.

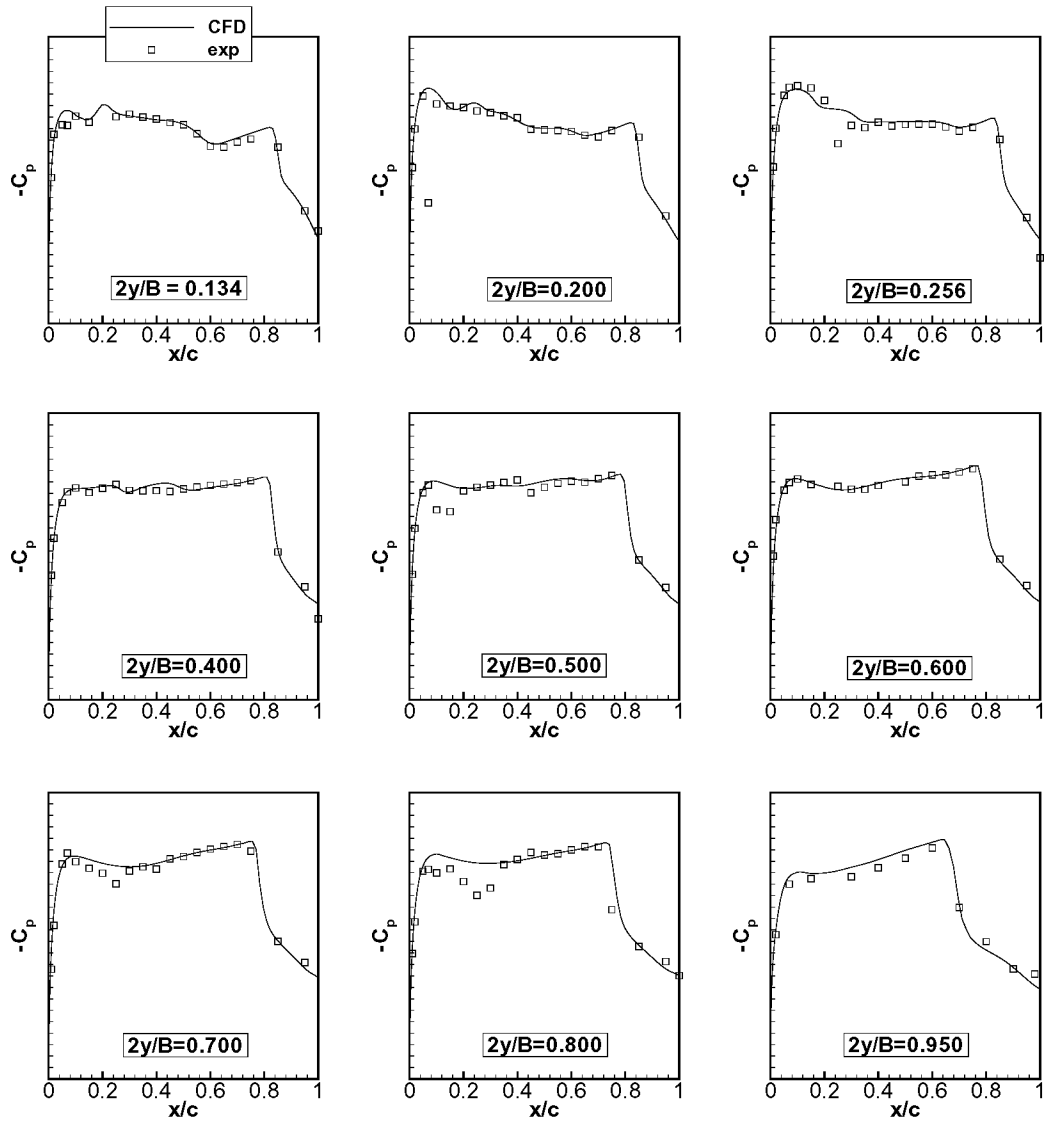


Figure 24: Predicted surface pressure coefficients at SS condition, OVERFLOW, SA model.

$\alpha = 2.5^\circ$ (BO-) through the buffet onset angle (BO) to $\alpha = 3.0^\circ$ (BO+) (runs 12, 5, and 11). The CFD consistently predicts the shock too far aft at the $2y/B = 0.70$ and 0.80 stations, but the forward movement of the shock with angle of attack agrees qualitatively with the experimental movement at all span stations.

Results at two higher angles of attack of $\alpha = 4.0^\circ$ and $\alpha = 5.1^\circ$ are shown in Figs. 27 and 28, respectively (wind tunnel model angle of attack in these cases is $\alpha = 4.1^\circ$ and 5.1°). Results are good at the inboard stations, but the CFD predicts the shock too far aft starting near mid-span, and the prediction gets progressively worse out to $2y/B = 0.80$. Very near the wing tip, however, the CFD predicted shock location is close to the experiment again.

Note the “dip” in the upper surface experimental pressures at $2y/B = 0.80$ between 15 - 40% chord in Figs. 21, 24, 25, 26, 27, and 28. It occurs at all angles of attack, but appears to be more exaggerated at the higher angles of attack. After some preliminary analysis, we believe that this dip is physical (i.e., not merely bad pressure taps). One piece of evidence in support of this belief is that the dip is a function of temperature (the dip increases with decreasing tunnel temperature). It is possible that at low temperatures a gap is opening at a model part break near this location. While this cause is only speculation at this time, it is possible that the experimental shock location was influenced by whatever is occurring in this region. Therefore, the CFD disagreement with experimental shock location should not carry any weight until more conclusive validations can be performed.

The computed lift, drag, and moment coefficients are compared to experiment in Figs. 29, 30, and 31. Included in these figures are *all* CFD results on the 7.1 million point grids, excluding Grid 4. Thus, the CFD “error band” due to code, differencing method, turbulence model, and tunnel aeroelastic effects are represented by the range of solutions shown at $\alpha = 2.8^\circ$. The results due to two particular codes and turbulence models are also plotted with thin broken lines. It is shown that CFL3D with EASM tends to yield higher lift levels, higher drag levels, and more negative moment levels than OVERFLOW with SA at all angles of attack. (Although not computed over a range of angles of attack, the SST or BB models are expected to yield lower lift levels, lower drag levels, and more positive moment levels than SA, based on results at the BO condition.) Note that solutions at $\alpha = 4.0^\circ$ and $\alpha = 5.1^\circ$ use Grid 3 (runs 20, 21, and 27). Aeroelastically-correct grids were not created for these angles of attack; however, because of the relative stiffness of the NTF model and based on differences due to aeroelastic effects at lower angles of attack, results are not expected to be much different.

These results indicate that the CFD is predicting the lift, drag, and moment levels from the experiment fairly well. Lift tends to be slightly overpredicted, and moment underpredicted (overpredicted in magnitude). The larger CFD error band in the moment is evident. Note in Figs. 29 and 31 the correlation between the change in lift curve slope (near $\alpha = 2^\circ$) and the pitching moment break. CFD results follow the experimental slope changes.

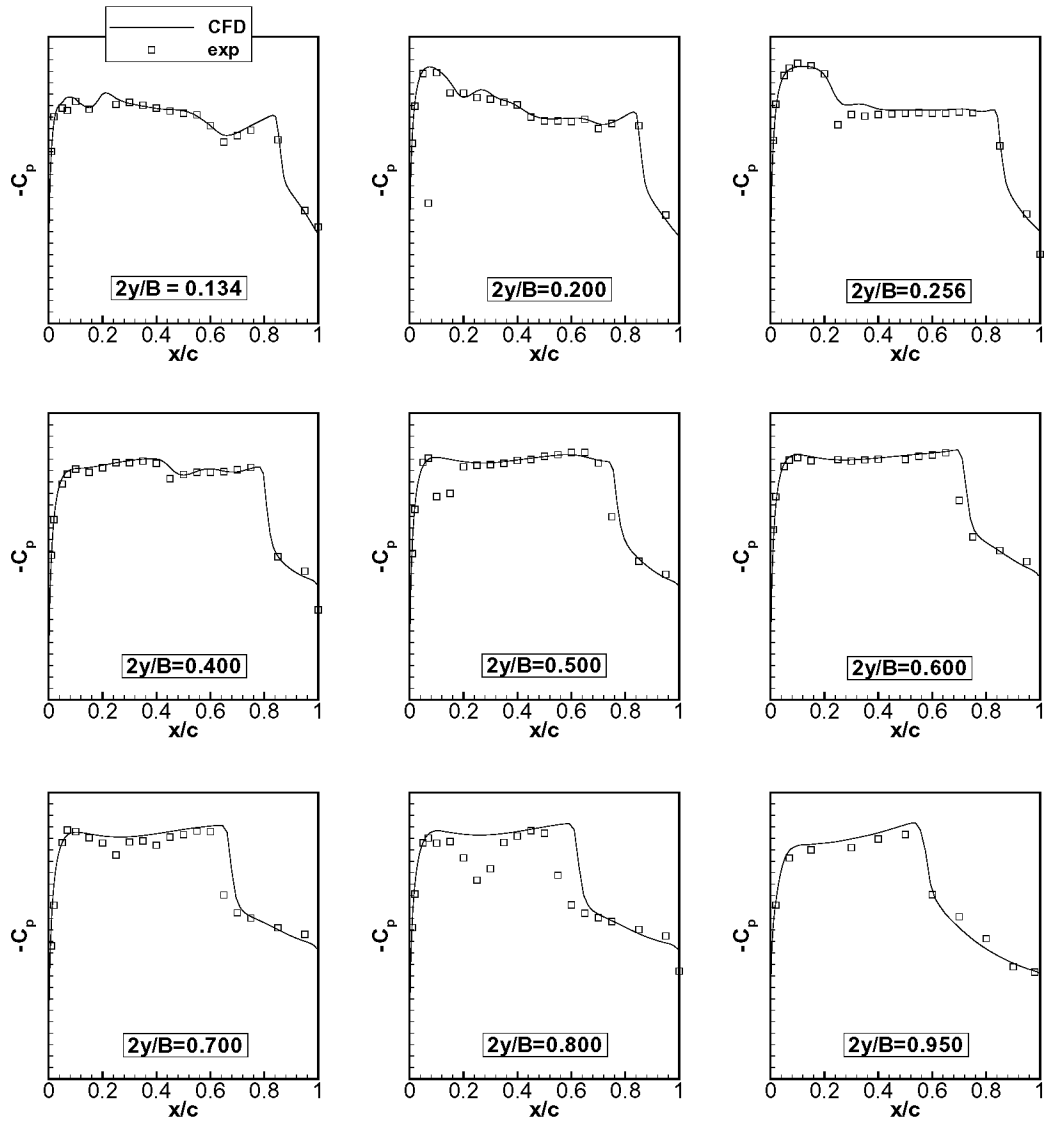


Figure 25: Predicted surface pressure coefficients at BO condition, OVERFLOW, SA model.

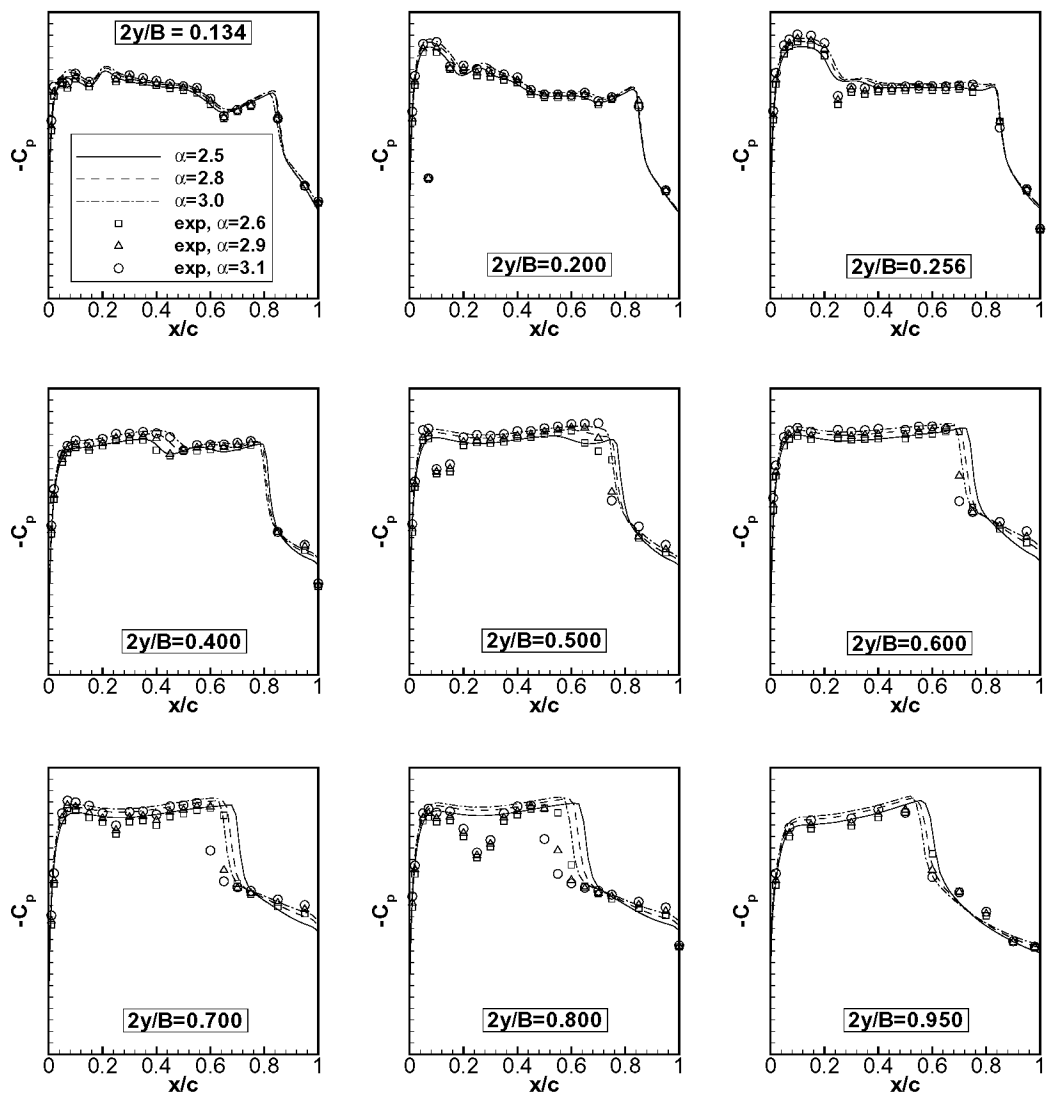


Figure 26: Range of surface pressure coefficients between $\alpha = 2.5^\circ$ and $\alpha = 3.0^\circ$ (BO-, BO, and BO+ conditions), OVERFLOW, SA model.

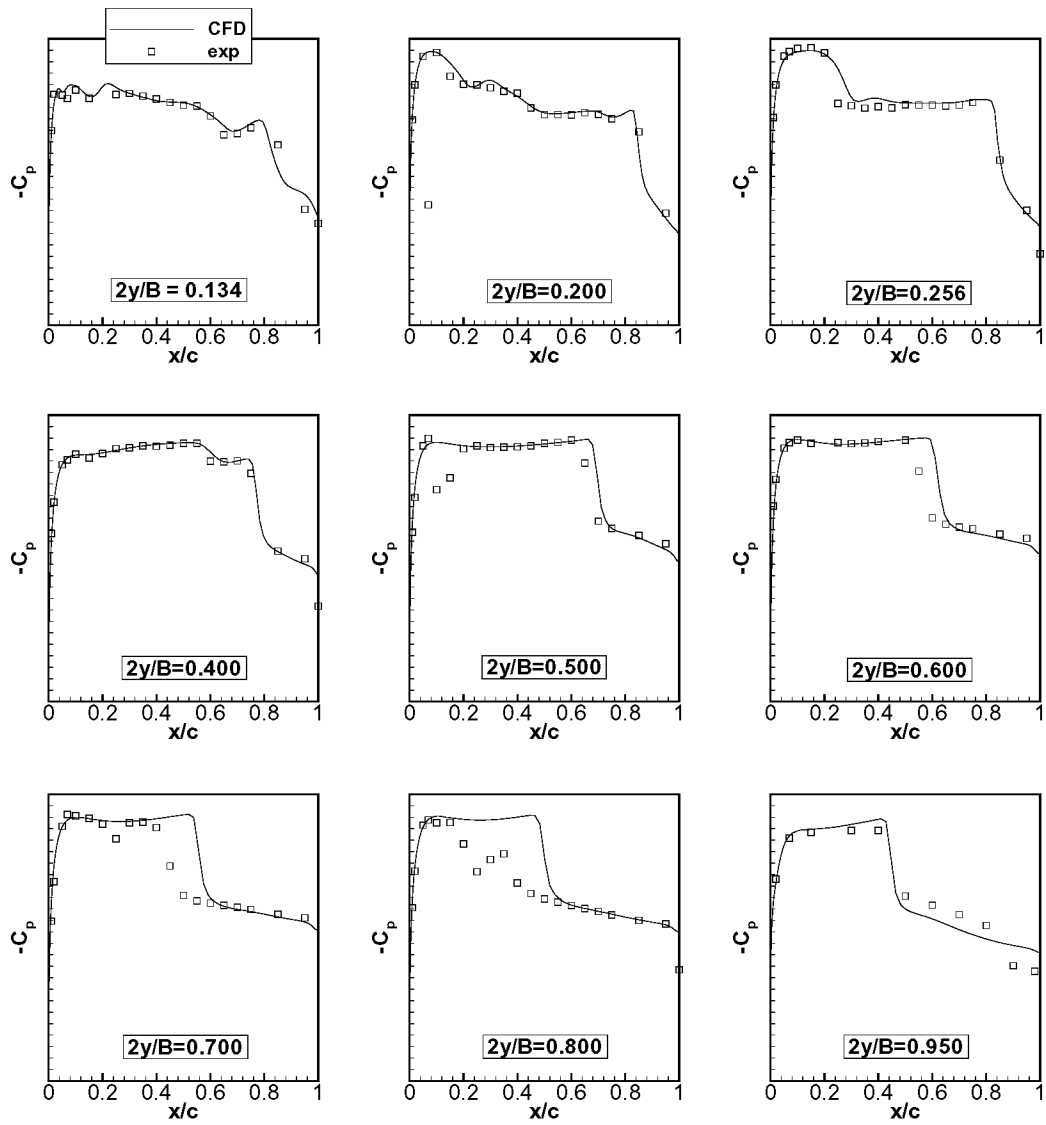


Figure 27: Predicted surface pressure coefficients at $\alpha = 4.0^\circ$ (past BO condition), OVERFLOW, SA model.

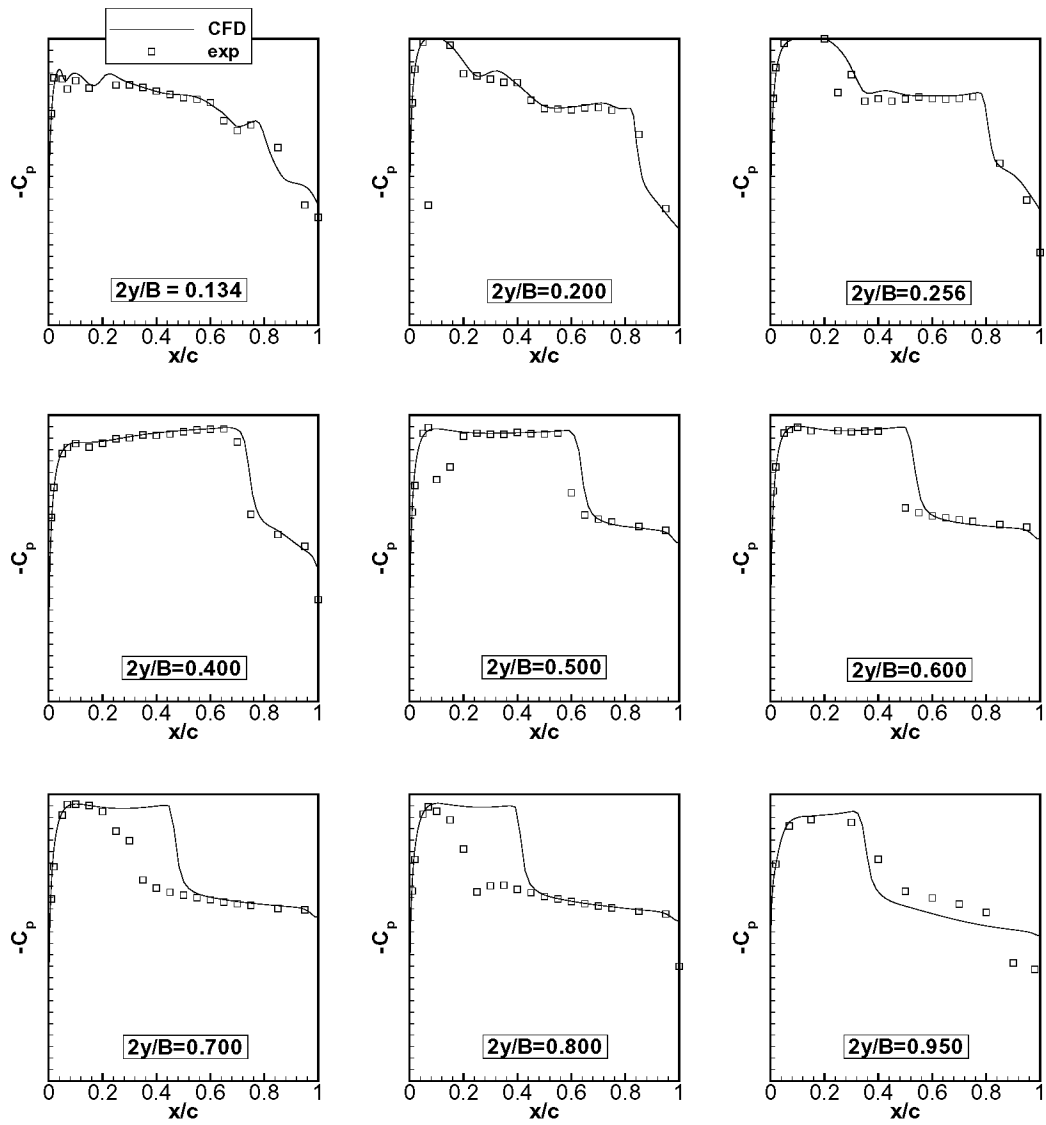


Figure 28: Predicted surface pressure coefficients at $\alpha = 5.1^\circ$ (past BO condition), OVERFLOW, SA model.

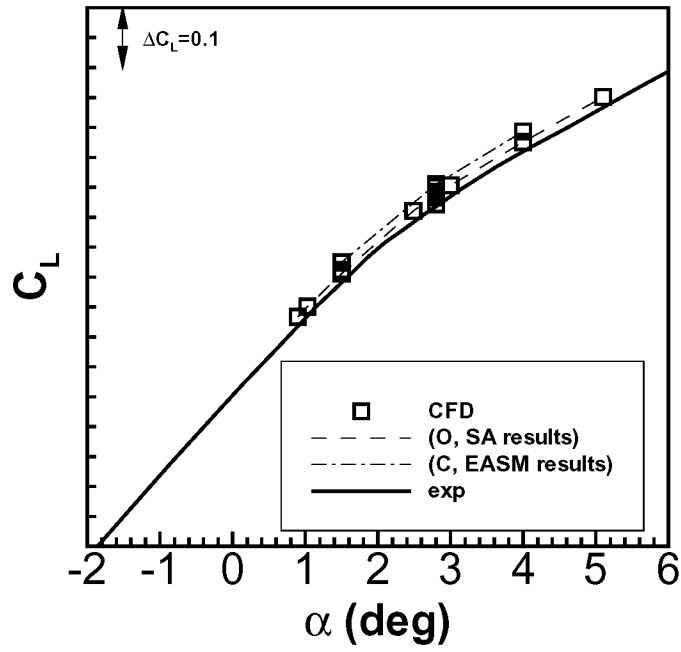


Figure 29: Lift coefficient comparisons.

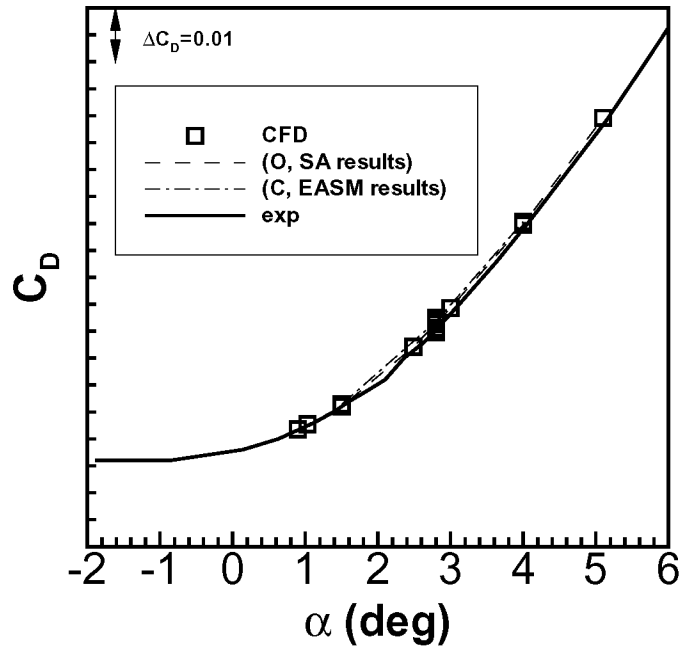


Figure 30: Drag coefficient comparisons.

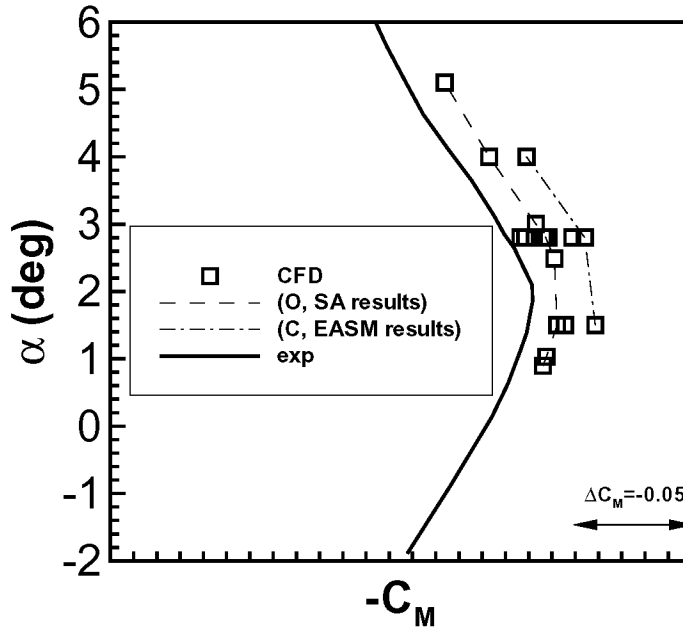


Figure 31: Moment coefficient comparisons.

5 COMPARISONS WITH FLIGHT DATA

5.1 Discussion on Flight Data

There is some uncertainty as to how to best compare flight test data with wind tunnel data and CFD, particularly for off-design conditions such as buffet onset. At the present time, buffet onset and the angle and lift at which it occurs in the wind tunnel is determined based on a heuristic methodology that makes use of force data trends. Buffet in flight is determined in a completely different manner, based on accelerometer readings (e.g., ± 0.05 g's at the pilot's seat). Also, most correlations between wind tunnel and flight data must contend with the difficult issue of Reynolds number scaling, because most wind tunnels operate at much lower Reynolds numbers than flight vehicles. Currently, the NTF and ETW are unique in their ability to achieve flight Reynolds numbers.

Even if one is fortunate enough to have the use of a wind tunnel that can be operated at flight Reynolds numbers, a major difficulty associated with comparing wind tunnel data with flight data directly is the fact that the tunnel model has very different aeroelastic characteristics from the flight vehicle: the scaled model is much stiffer. The wind tunnel model is designed so that its deflected shape matches the deflected shape of the flight vehicle at cruise Mach number and Reynolds number. However, at any other conditions outside of cruise, the two shapes do not match. Building additional wind tunnel models to match flight aeroelastics at different conditions is not practical, so instead a process termed “rigidification” was developed by aircraft manufacturers as a method to compare different data sets (see section 1.2). In the rigidification process, the flight force curve is modified to approximate what it would be

if aeroelastic deflections were removed from the actual wing. For example, if the force curve is rigidified about its 1-g shape, then the resulting curve is intended to be what would result if the wing could remain frozen at its 1-g shape throughout the angle of attack sweep. The problem with the rigidification process is that it utilizes linear scaling techniques, which have questionable validity in regions outside of the point about which the linearization is being taken.

CFD often uses only one grid throughout an entire angle of attack sweep. This is tantamount to ignoring aeroelastic effects. However, if the flight aeroelastic shapes are known, it is a relatively easy task (certainly simpler and less expensive than building different wind tunnel models) to create an appropriate grid for each angle of attack and avoid altogether the need for rigidified flight data to compare against. For the current study, linear aerodynamics in combination with a finite element model were used to derive an *estimate* of the wing's aeroelastic shape. This was only done for conditions near flight buffet onset.

There are other uncertainties associated with flight data as well. The actual body angle of attack in flight can be uncertain, due to body aeroelastics which can be significant for the flight vehicle. Also, there is not a single set of flight force curves because they depend on flight conditions such as aircraft weight, fuel distribution, altitude, thrust effects, etc. Some of these conditions are not accounted for in CFD simulations or wind tunnel tests. Finally, the validity of pressure data from flight for CFD or wind tunnel comparison is questionable because, at off-design conditions, flight data is often obtained through unsteady maneuvers. These maneuvers can yield inconsistent results between the inside and outside wings, and can also present other difficulties in interpretation when compared to steady wind tunnel or CFD results.

In the case of the current aircraft, the flight vehicle has vortex generators (VGs) on the wings. The VGs have little to no effect near cruise conditions, but can significantly reduce the amount of separated flow at higher angles of attack. Wind tunnel tests have been run both with and without VGs. The VGs can be modeled in CFD as well, but doing so is more difficult for grid generation and much more expensive for the flow solver due to the larger number of required grid points.

Finally, wind tunnel models and CFD are often run with no horizontal tail. In this case, the flight data results are “de-trimmed” to compare with the wind tunnel data. Although there is more confidence in this process than in the rigidification process for some conditions, it represents an additional step of altering the original flight data before comparing with wind tunnel data or CFD. When combined with other modifications, this de-trimming has the potential for introducing still more uncertainty into the comparisons.

In the following section, CFD data is compared with de-trimmed elastic flight data curves, extracted from a flight simulator. *However, the comparison should be viewed qualitatively only.* Although not shown, several sets of flight data were extracted at different times, and there are unexplained variations and inconsistencies between them. These inconsistencies do not indicate any problems with the flight data itself, but rather point out the difficulties associated with comparing flight data from a simulator with wind tunnel data or CFD. The goal of the simulator process is to faithfully approximate flight conditions and characteristics. It was never intended for comparison to wind tunnel data or CFD. It is clearly difficult to know what to extract from the flight simulator for direct comparisons; there is a lot of variability possible, depending on how it is done. Therefore, the elastic flight data shown in the next section is used to note trends only, and *not* to establish absolute levels.

Table 4: VG increments from wind tunnel data applied to CFD lift and moment

α , deg	ΔC_L	ΔC_M
2.8	0.025	-0.028
4.0	0.04	-0.045
5.1	0.05	-0.045
7.0	unknown	unknown
9.0	unknown	unknown

5.2 Comparisons

Three grids (grids 1, 3, and 4) were used in the comparison of CFD with flight data. Grid 1 was used for computed results at $\alpha = 1.03^\circ$ because the NTF wing shape at OC conditions is believed to be close to that of the flight vehicle in flight at the same conditions. Grid 3 corresponds with the wind tunnel model shape at $\alpha = 2.8^\circ$, and Grid 4 is an approximate flight shape at buffet onset based on a linear loads analysis, as discussed in detail in earlier sections. Furthermore, all grids are based on the wind tunnel model, so their trailing edges are slightly thicker (scaled) than the flight vehicle. There are no VGs or FSFs modeled in the grids, and there is no horizontal or vertical tail.

Grid 4 was run at a variety of angles of attack, from $\alpha = 2.8^\circ$ through $\alpha = 9^\circ$ (runs 17, 22, 23, 24, 25). Obviously, the aeroelastics of the flight vehicle play a significant role throughout this large a range. The Grid 4 itself is believed to approximately represent the actual wing shape only somewhat near flight buffet onset conditions. Its validity at other angles of attack is unknown. Grid 3 was run at three angles of attack (runs 5, 20, 21) in order to determine the effect of the relatively large aeroelastic shape difference between grids 3 and 4 on the forces and moments.

Computed lift is compared to flight data in Fig. 32, and moment is compared in Fig. 33. Because VGs were not modeled in the CFD, their effect, which is known to be important for conditions with upper surface wing separated flow, was approximately accounted for in these plots; wind tunnel experiments that investigated the effects of VGs on lift and moment were used to establish approximate increments. There is some confidence in this wind tunnel procedure based on earlier successes predicting VG increments for a different aircraft, which had flight data both with and without VGs to compare against [25]. For the present CFD data, the lift and moment increments applied are given in Table 4.

As discussed earlier, the results in Figs. 32 and 33 should be viewed with caution. Data from the flight simulator in this case is suspect: for example, near $\alpha = 1^\circ$ (1-g conditions), the flight data is significantly lower in absolute level than expected. However, viewing the comparison *qualitatively*, the CFD results follow the lift curve trend well through buffet onset to maximum lift. There is no evidence here of CFD tailing off prior to flight buffet levels, as was reported for other aircraft (see Appendix A). The moment curve shows greater deviation from the flight results, but this is a more sensitive quantity than the lift, and the potential variability of the extracted flight data from the simulator is larger. The effects of the aeroelastic shape differences between grids 3 and 4 are relatively minor (roughly 0.02 in C_L and 0.01 in C_M); they do not cause any dramatic changes in the lift or moment curve behavior.

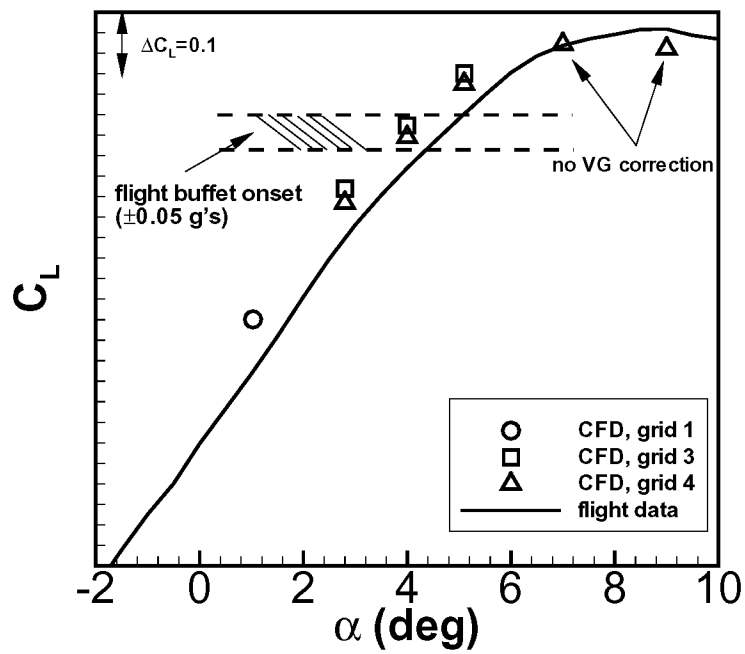


Figure 32: Comparison of computed lift with elastic flight data, OVERFLOW, SA model (grid 1 = OC NTF model, grid 3 = BO NTF model, grid 4 = BOF estimated flight vehicle).

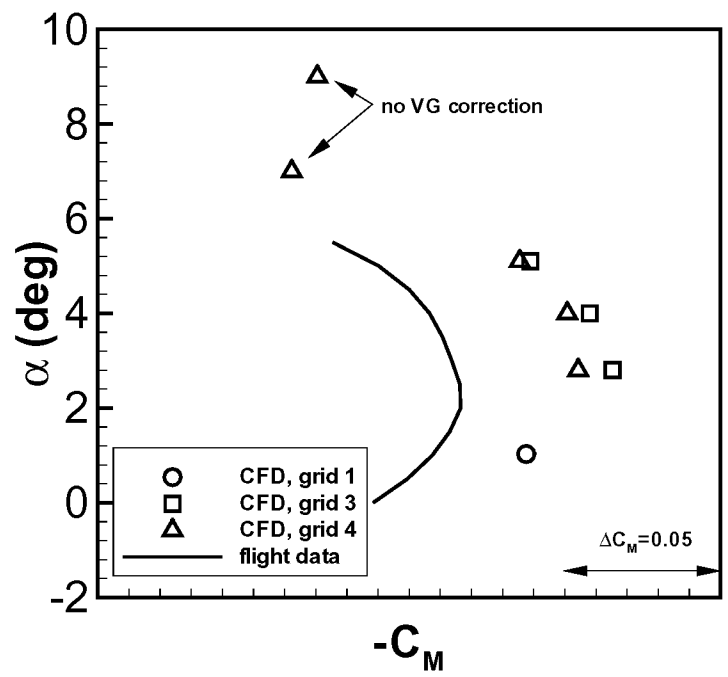


Figure 33: Comparison of computed moment with elastic flight data, OVERFLOW, SA model (grid 1 = OC NTF model, grid 3 = BO NTF model, grid 4 = BOF estimated flight vehicle).

6 SUMMARY

In this report, results from the NASA-Boeing CFD Buffet Onset Team were presented. This team was created to investigate reported problems with state-of-the-art CFD applied to flows over aircraft configurations with significant regions of separated flow. Specifically, the team was motivated by the fact that previous CFD results and wind tunnel experiments for other aircraft have underpredicted buffet onset lift levels compared to flight test results. The team focused on flow over a modern civil transport at $M = 0.87$ (overspeed) at buffet-onset conditions. The rationale behind this choice was discussed.

Current CFD capabilities and known limitations were outlined. Three potential sources of error in CFD computations – numerical errors, geometric fidelity, and turbulence model – were discussed as a background to the current problem. The methodology employed in the current study was described.

Based on the team goal to establish the sensitivities due to grid, turbulence model, code, etc., for the current aircraft in buffet/separated conditions, the primary focus of this paper was a CFD sensitivity analysis. The effects of grid density and grid extent were established for buffet onset; use of an overset grid with 7.1 million points was in error from an infinite density grid by less than 1% in lift and drag, and less than 3% in moment. Results using a far field extent of 25 MAC was different from results using 50 MAC by less than 0.1% in forces and moment.

The effects of code and spatial differencing method were also explored. The effect of code was the greater effect: 2% difference in lift, 2% in drag, and 6% in moment on the grid with 7.1 million points. The effect of differences in wind tunnel model aeroelastic shape was fairly small (0.7% in lift, 2.4% in drag, 0.7% in moment), but the difference between results using a wind tunnel shape vs. using an estimated *flight* vehicle shape was large (4% in lift, 11% in drag, 6% in moment).

The effect of four different turbulence models was assessed. Two of these models – SA and SST – represent state-of-the-art models in wide use currently throughout the world for both attached and separated aerodynamic flows. EASM is a more recently-developed nonlinear model that is derived directly from the full second-moment Reynolds stress model. The BB model was also assessed, although it has lost favor in the CFD community due to potential problems near boundary layer edges. For a given code using the grid with 7.1 million points, the maximum difference between turbulence model results was approximately 3% in lift, 4% in drag, and 8% in moment.

In summary, given a grid of sufficient density for a given aeroelastic wing shape, the combined approximate error band in CFD due to code, spatial differencing method, and turbulence model is: 6% in lift, 7% in drag, and 16% in moment. The biggest two contributors to this uncertainty are turbulence model and code.

Comparisons were made with wind tunnel data. Computed results agreed well with surface pressure measurements both for an overspeed “cruise” case as well as a case with small trailing edge separation. At and beyond buffet onset, computed results agreed well over the inner half of the wing, but shock location was predicted too far aft at most of the outboard stations. However, a “dip” in experimental surface pressures at one of the outboard stations may indicate a gap opening in the configuration at low temperatures; this could influence the experimental shock location. Nonetheless, computed lift and moment curves were predicted in good agreement with experimental results from the wind tunnel.

The pedigree of flight data from a simulator program was discussed, including issues surrounding a rigidification process. Potential problems in using simulator-generated data for comparison with wind tunnel data and CFD were highlighted. While lift curves from current CFD results do show the characteristic lift curve “break” near buffet onset, they show no indication of reaching maximum lift prior to flight buffet levels: the CFD curves follow the flight lift curve trend well past buffet to maximum lift. It should be emphasized, however, that the off-design flight wing shape is unknown (not measured). The flight shape at buffet used in the CFD was estimated using a loads analysis. Therefore, the actual load distribution is unknown, and detailed comparisons of CFD computations with flight data should be viewed with caution.

7 CONCLUDING REMARKS

The current effort was motivated by a problem identified by the U.S. aircraft industry: that state-of-the-art CFD (specifically, Reynolds-averaged Navier-Stokes with current turbulence models) cannot adequately or consistently predict separated flows. In particular, a specific issue was identified: CFD (and wind tunnel experiment) have predicted lower buffet lift levels than experienced in flight for two aircraft. In fact, CFD and wind tunnel did not even *achieve* flight lift levels near flight buffet onset.

Prior to the initiation of the current study, some data for the current aircraft suggested a similar trend. At Mach numbers above nominal cruise, wind tunnel data showed a lower buffet C_L than for flight. The current effort was undertaken using a modern civil transport in order to (1) attempt to reproduce the problem seen for other aircraft, and (2) try to identify the underlying cause(s) of the discrepancy. As an integral part of this effort, the CFD sensitivities due to grid, code, spatial differencing method, aeroelastic shape, and turbulence model were established for the current aircraft near buffet onset.

The bottom line of the investigation is that the problem of CFD being unable to achieve flight buffet levels did *not* occur for the current aircraft. Instead, the predicted lift curve from CFD tracked the trend from flight data well through buffet all the way to near maximum lift. If anything, the relatively small error band due to two different codes and four different turbulence models for a separated flow buffet-onset case, combined with good agreement with experiment, suggests some validity of today's state-of-the-art CFD tools for aerodynamic flows outside of the cruise envelope.

The reasons for the success of CFD in this case as opposed to the failure of CFD in earlier studies are not known. It is possible that the flow fields of the configurations in the earlier studies are more sensitive to small perturbations near buffet onset than the flow field of the current configuration. Part of the difference may also be due to the use of inappropriate flight data: the use of simulator-derived flight data as well as the use of a rigidification process appear to be questionable for comparing to wind tunnel or CFD results. Finally, many of the geometric simplifications and omissions necessary when performing CFD analysis of a complex flight vehicle are a potential source of error.

It is clear that in spite of advances in CFD over the last 20 years, its use remains far from "push button" at the present time. Particularly for complex configurations and for flows outside of the cruise envelope, a significant amount of user knowledge and experience is required to successfully apply CFD, both in the grid generation as well as in the flow solution phases. Over time, as CFD is applied to an increasing number of configurations, and as U.S. industry continues to incorporate CFD into its design processes, CFD codes and methodologies will improve and reduce the risk associated with running complex off-design cases. Improved error analysis is also expected to increase confidence in CFD results.

Certainly, turbulence modeling remains an active area of research. Today's turbulence models remain far from perfect, and there are doubtless many situations for which any given model can produce poor or even incorrect results. However, the current study has failed to identify any particular turbulence model failure. In any case, it is doubtful that failure in a complex configuration case would lead to any insight into a specific turbulence model deficiency, because so many other potential sources of error exist. Usually, only through well-designed, simple unit problem experiments and CFD analysis can improvements to turbulence models be made.

ACKNOWLEDGMENTS

The authors gratefully acknowledge Roger Clark and Deepak Om of Boeing, and Richard Wahls and James Thomas of NASA, for their sponsorship and guidance during the course of this investigation.

APPENDIX A: INDUSTRY PERSPECTIVE ON CFD

This appendix summarizes, in bullet form, some of the major observations and conclusions made in the Boeing-proprietary talk “CFD Successes and Challenges.” Most of this material resulted from studies funded through NASA’s Advanced Subsonic Transport (AST) program. This summary serves as a backdrop for the current study. Primarily, three different CFD codes were used to generate these observations and conclusions: CFL3D, OVERFLOW, and TLNS3D. The first two are the same codes used in the current study. TLNS3D is a central-difference code [26]. Also, the Johnson-King turbulence model [27] is mentioned; this model was not used in the current study.

The first part of the list includes general observations or lessons learned:

- 2-D airfoil testing is not really 2-D, even when there is sidewall suction: For example, CFD misses trends and shock location for a high-wing transport type airfoil. CFD results improve if run in 3-D and sidewall suction present in the experiment is modeled.
- When modeling thick trailing edge wings, it is better to “close the wake” with the grid (many CFD users opt to leave a gap in the wake – this improves convergence, but also adversely affects shock location and misrepresents possible real unsteady physics).
- Upwind differencing is generally recommended over central differencing. Central differencing tends to smear shocks, underpredict suction peaks, and overshoot total pressure.
- The Baldwin-Barth turbulence model exhibits problems (kinks) near the edge of boundary layers that get worse with grid refinement.
- There are inherent difficulties comparing CFD with low Reynolds number wind tunnel data because of uncertainty of transition location on the tunnel model.
- CFD is not reliable for estimating flight Reynolds number aileron effectiveness characteristics when flow separation is involved.
- For airframe/engine integration, CFD enables the design of interference-drag-free installations, and gives excellent insight into Reynolds number scaling effects for attached flows; but there is less confidence for predicting separated flows.
- Actual digitized (as-built) geometry can be different from a design shape; using CFD with the digitized geometry improves comparison with experiment.
- Including the sting in a CFD simulation can be important for some wing/body configurations: it can affect shock location on the wing.

The second part of the list includes more specific results, for particular configurations:

- For several modern wings and aircraft configurations near cruise conditions, CFD with the Spalart-Allmaras turbulence model yields excellent agreement with NTF experiment.
- For a particular wing near buffet onset, CFD with Spalart-Allmaras is in fair agreement with NTF experiment (worst near tip – shock too far aft), and fairly closely follows experimental C_L - α trend. The Johnson-King turbulence model predicts the shock significantly too far aft, and gives much too high C_L at buffet. For a different wing near buffet onset, CFD with Spalart-Allmaras is in excellent agreement with NTF experiment.

- For a particular application with a winglet, CFD does not capture the pattern of the separated juncture flow.
- For a tri-engine civil transport, CFD with Spalart-Allmaras closely follows NTF C_L - α trend, which breaks too early compared with corrected flight data (i.e., flight buffet occurs at higher lift than CFD or wind tunnel experiment).
- For a high-wing transport (HWT), CFD is close to NTF data, which again breaks too early, and does not look like it can reach flight buffet onset levels. At lower angles of attack, C_p predictions agree well with NTF. At higher angle of attack, results are generally good, except at a mid-span location where CFD shock location is forward of NTF.
- For a HWT wing alone, Johnson-King turbulence model gives higher lift than Spalart-Allmaras, particularly at high angles of attack, where Spalart-Allmaras tends to break and Johnson-King tends to keep increasing (*Note: this behavior induces the speculation that Johnson-King might predict full-configuration flight trends better than Spalart-Allmaras – however, Johnson-King has inherent limitations which makes it problematic for coding in a general multi-zone CFD code*).

References

- [1] Menter, F. R., “Improved Two-Equation k - ω Turbulence Models for Aerodynamic Flows,” NASA TM 103975, Oct. 1992.
- [2] Spalart, P. R., and Allmaras, S. R., “A One-Equation Turbulence Model for Aerodynamic Flows,” *La Recherche Aeronautique*, No. 1, 1994, pp. 5–21.
- [3] Baldwin, B. S., and Lomax, H., “Thin-Layer Approximation and Algebraic Model for Separated Turbulent Flows,” AIAA Paper 78-257, Huntsville, AL, 1978.
- [4] Wilcox, D. W., Turbulence Modeling For CFD, DCW Industries, Inc., 1994.
- [5] Gatski, T. B., and Speziale, C. G., “On Explicit Algebraic Stress Models for Complex Turbulent Flows,” *Journal of Fluid Mechanics*, Vol. 254, 1993, pp. 59–78.
- [6] Rumsey, C. L., and Gatski, T. B., “Recent Turbulence Model Advances Applied to Multi-element Airfoil Computations,” AIAA Paper 2000-4323, Denver, CO, 2000.
- [7] Rumsey, C. L., Sanetrik, M. D., Biedron, R. T., Melson, N. D., and Parlette, E. B., “Efficiency and Accuracy of Time-Accurate Turbulent Navier-Stokes Computations,” *Computers and Fluids*, Vol. 25, No. 2, 1996, pp. 217–236.
- [8] Wang, D., Wallin, S., Berggren, M., Eliasson, P., “A Computational Study of Unsteady Turbulent Buffet Aerodynamics,” AIAA Paper 2000-2657, Denver, CO, 2000.
- [9] Garner, P. L., Meredith, P. T., Stoner, R. C., “Areas for Future CFD Development as Illustrated by Transport Aircraft Applications,” AIAA Paper 91-1527-CP, Honolulu, HI, 1991.
- [10] Rogers, S. E., Roth, K., Cao, H. V., Slotnick, J. P., Whitlock, M., Nash, S. M., and Baker, M. D., “Computation of Viscous Flow for a Boeing 777 Aircraft in Landing Configuration,” AIAA Paper 2000-4221, Denver, CO, 2000.

- [11] Clark, R. W., Pelkman, R. A., “High Reynolds Number Testing of Advanced Transport Aircraft Wings in the National Transonic Facility,” AIAA Paper 2001-0910, Reno, NV, 2001.
- [12] Burner, A., Liu, T., Garg, S., Ghee, T., Taylor, N., “Aeroelastic Deformation Measurement Technique for Slotted Flaps on Wind Tunnel Models,” AIAA Paper 2000-2386, Denver, CO, 2000.
- [13] Jiang, F., “CFD Predictions for Control Surface Effectiveness,” AIAA Paper 2000-0510, Reno, NV, 2000.
- [14] McDonnell Douglas Aerospace, “Integrated Wing Design, Technology Integration & Environmental Impact Wing Design / PAI,” Technical progress report for NASA contract NAS1-20268, December 18, 1996.
- [15] McDonnell Douglas Aerospace, “Integrated Wing Design, Technology Integration & Environmental Impact Wing Design / PAI,” Technical progress report for NASA contract NAS1-20268, February 13, 1997.
- [16] Krist S. L., Biedron R. T., and Rumsey C. L., “CFL3D User’s Manual (Version 5.0)”, NASA TM-1998-208444, June 1998.
- [17] Jespersen, D. C., Pulliam, T. H., and Buning, P. G., “Recent Enhancements to OVERFLOW,” AIAA Paper 97-0644, Reno, NV, 1997.
- [18] Suhs, N. E. and Tramel, R. W., “PEGSUS 4.0 User’s Manual,” Arnold Engineering Development Center Report AEDC-TR-91-8, November 1991.
- [19] Baldwin, B. S. and Barth, T. J., “A One-Equation Turbulence Transport Model for High Reynolds Number Wall-Bounded Flows,” NASA TM-102847, August, 1990.
- [20] Menter, F. R., “Eddy Viscosity Transport Equations and their Relation to the $k-\varepsilon$ Model,” *Journal of Fluids Engineering*, Vol. 119, No. 12, 1997, pp. 876–884.
- [21] Menter, F. R., “Two-Equation Eddy-Viscosity Turbulence Models for Engineering Applications,” *AIAA Journal*, Vol. 32, No. 8, 1994, pp. 1598–1605.
- [22] Menter, F. R., Rumsey, C. L., “Assessment of Two-Equation Turbulence Models for Transonic Flows,” AIAA Paper 94-2343, Colorado Springs, CO, 1994.
- [23] Rumsey, C. L., Vatsa, V. N., “Comparison of the Predictive Capabilities of Several Turbulence Models,” *Journal of Aircraft*, Vol. 32, No. 3, 1995, pp. 510–514.
- [24] Abid, R., Rumsey, C. L., Gatski, T. B., “Prediction of Nonequilibrium Turbulent Flows with Explicit Algebraic Stress Models,” *AIAA Journal*, Vol. 33, No. 11, 1995, pp. 2026–2031.
- [25] Wahls, R. A., “The National Transonic Facility: A Research Retrospective,” AIAA Paper 2001-0754, Reno, NV, 2001.
- [26] Vatsa, V. N., Sanetrik, M. D., Parlette, E. B., Eiseman, P., and Cheng, Z., “Multi-block Structured Grid Approach for Solving Flows over Complex Aerodynamic Configurations,” AIAA Paper 94-0655, Reno, NV, 1994.
- [27] Johnson, D. A. and Coakley, T. J., “Improvements to a Nonequilibrium Algebraic Turbulence Model,” *AIAA Journal*, Vol. 28, No. 11, 1990, pp. 2000–2003.

REPORT DOCUMENTATION PAGE			Form Approved OMB No. 0704-0188	
Public reporting burden for this collection of information is estimated to average 1 hour per response, including the time for reviewing instructions, searching existing data sources, gathering and maintaining the data needed, and completing and reviewing the collection of information. Send comments regarding this burden estimate or any other aspect of this collection of information, including suggestions for reducing this burden, to Washington Headquarters Services, Directorate for Information Operations and Reports, 1215 Jefferson Davis Highway, Suite 1204, Arlington, VA 22202-4302, and to the Office of Management and Budget, Paperwork Reduction Project (0704-0188), Washington, DC 20503.				
1. AGENCY USE ONLY (Leave blank)	2. REPORT DATE December 2001	3. REPORT TYPE AND DATES COVERED Technical Memorandum		
4. TITLE AND SUBTITLE CFD Sensitivity Analysis of a Modern Civil Transport Near Buffet-Onset Conditions			5. FUNDING NUMBERS WU 706-21-11-10	
6. AUTHOR(S) Christopher L. Rumsey, Dennis O. Allison, Robert T. Biedron, Pieter G. Buning, Thomas G. Gainer, Joseph H. Morrison, S. Melissa Rivers, Stephen J. Mysko, and David P. Witkowski				
7. PERFORMING ORGANIZATION NAME(S) AND ADDRESS(ES) NASA Langley Research Center Hampton, VA 23681-2199			8. PERFORMING ORGANIZATION REPORT NUMBER L-18133	
9. SPONSORING/MONITORING AGENCY NAME(S) AND ADDRESS(ES) National Aeronautics and Space Administration Washington, DC 20546-0001			10. SPONSORING/MONITORING AGENCY REPORT NUMBER NASA/TM-2001-211263	
11. SUPPLEMENTARY NOTES Rumsey, Allison, Biedron, Buning, Gainer, Morrison, and Rivers: Langley Research Center, Hampton, VA; Mysko, The Boeing Company, Long Beach, CA; Witkowski, The Boeing Company, Seattle, WA.				
12a. DISTRIBUTION/AVAILABILITY STATEMENT Unclassified-Unlimited Subject Category 02 Distribution: Nonstandard Availability: NASA CASI (301) 621-0390			12b. DISTRIBUTION CODE	
13. ABSTRACT (Maximum 200 words) A CFD sensitivity analysis is conducted for a modern civil transport at several conditions ranging from mostly attached flow to flow with substantial separation. Two different Navier-Stokes computer codes and four different turbulence models are utilized, and results are compared both to wind tunnel data at flight Reynolds number and flight data. In-depth CFD sensitivities to grid, code, spatial differencing method, aeroelastic shape, and turbulence model are described for conditions near buffet onset (a condition at which significant separation exists). In summary, given a grid of sufficient density for a given aeroelastic wing shape, the combined approximate error band in CFD at conditions near buffet onset due to code, spatial differencing method, and turbulence model is: 6% in lift, 7% in drag, and 16% in moment. The biggest two contributors to this uncertainty are turbulence model and code. Computed results agree well with wind tunnel surface pressure measurements both for an overspeed "cruise" case as well as a case with small trailing edge separation. At and beyond buffet onset, computed results agree well over the inner half of the wing, but shock location is predicted too far aft at some of the outboard stations. Lift, drag, and moment curves are predicted in good agreement with experimental results from the wind tunnel.				
14. SUBJECT TERMS Separated flow; Variability; Turbulence model			15. NUMBER OF PAGES 62	
			16. PRICE CODE	
17. SECURITY CLASSIFICATION OF REPORT Unclassified	18. SECURITY CLASSIFICATION OF THIS PAGE Unclassified	19. SECURITY CLASSIFICATION OF ABSTRACT Unclassified	20. LIMITATION OF ABSTRACT UL	